J. Fluid Mech. (2009), *vol.* 636, *pp.* 59–89.
doi:10.1017/S0022112009007939

Multiple asymptotic solutions for axially travelling waves in porous channels

JOSEPH MAJDALANI†

Mechanical, Aerospace and Biomedical Engineering Department, University of Tennessee Space Institute, 411 B. H. Goethert Parkway, Tullahoma, TN 37388-9700, USA

(Received 24 August 2008; revised 21 April 2009; accepted 4 May 2009)

Travelling waves in confined enclosures, such as porous channels, develop boundary layers that evolve over varying spatial scales. The present analysis employs a technique that circumvents guessing of the inner coordinate transformations at the forefront of a multiple-scales expansion. The work extends a former study in which a two-dimensional oscillatory solution was derived for the rotational travelling wave in a porous channel. This asymptotic solution was based on a free coordinate that could be evaluated using Prandtl's principle of matching with supplementary expansions. Its derivation required matching the dominant term in the multiple-scales expansion to an available Wentzel-Kramers-Brillouin (WKB) solution. Presently, the principle of least singular behaviour is used. This approach leads to a multiple-scales approximation that can be obtained independently of supplementary expansions. Furthermore, a procedure that yields different types of WKB solutions is described and extended to arbitrary order in the viscous perturbation parameter. Among those, the WKB expansion of type I is shown to exhibit an alternating singularity at odd orders in the perturbation parameter. This singularity is identified and suppressed using matched asymptotic tools. In contrast, the WKB expansion of type II is found to be uniformly valid at any order. Additionally, matched asymptotic, WKB and multiple-scales expansions are developed for several test cases. These enable us to characterize the essential vortico-acoustic features of the axially travelling waves in a porous channel. All solutions are numerically verified, compared and discussed.

1. Introduction

The modelling of axially travelling oscillatory waves in injection-driven porous chambers emerges as a necessity in several physical contexts. These include the analysis of acoustic instability, propellant gasification in solid rocket motors, surface ablation, filtration, water hammering and biological transport. The types of waves considered here may be induced externally, through the use of wave generators, or internally, due to the intrinsic coupling with the chamber's natural frequencies. Examples of the forced type are showcased in experimental investigations by Brown *et al.* (1986), Dunlap *et al.* (1990), Ma, Van Moorhem & Shorthill (1991) and Barron, Majdalani & Van Moorhem (2000). These are chiefly motivated by the need to capture the wave structure and potential instability during the burning of solid propellant grains. In this vein, cold-flow facilities are built to permit flow visualization and data acquisition in a safe environment. This is accomplished by allowing either the injection

† Email address for correspondence: maji@utsi.edu

of an inert gas across sintered metal plates or the expulsion of carbon dioxide from sublimating blocks of dry ice. The ensuing oscillatory motion is controlled through the use of rotating valves or four-bar linkages attached to a reciprocating piston. Procedurally, Ma *et al.* (1991) and Barron *et al.* (2000) follow Richardson & Tyler (1929) in adjusting the speed of their electric motors to the extent of controlling the reciprocating frequency of a piston mounted at the end of a crank.

The investigation of intrinsic self-induced oscillations is separately pursued and then summarized in two surveys by Ugurtas *et al.* (2000) and Fabignon *et al.* (2003). These discuss an innovative experimental facility known as *Veine d'Etude de la Couche Limite Acoustique* (VECLA). Casalis, Avalon & Pineau (1998) describe VECLA as a long rectangular channel with counterfacing porous and impervious walls. By injecting air uniformly along the porous side, inevitable fluctuations in the injection rate give rise to a well-defined acoustic environment that is accompanied by rich travelling wave structures. These are further discussed in a unifying study by Griffond (2002).

For a porous channel driven by sidewall mass injection, the travelling wave motion, excluding hydrodynamic instability waves, is treated by Majdalani (2001). For small-amplitude pressure oscillations, asymptotic formulations for the flow variables are obtained using three perturbation schemes. The undisturbed state is represented by an arbitrary mean-flow satisfying Berman's classic equation (Berman 1953; 1958), while symmetric time-dependent solutions are derived from the linearized vorticity and momentum transport equations. In short, a time-dependent laminar-flow approximation is extracted from the vorticity transport equation, and two other solutions are retrieved from the momentum equation using zeroth-order WKB and multiple-scales expansions (Majdalani 2001). Despite their dissimilar expressions, the three asymptotic solutions are found to agree with one another, with experiments and with numerical simulations of the nonlinear Navier–Stokes equations. One of the resulting formulations is later employed by Griffond (2002) in his study of hydrodynamic instability and wave propagation in an injecting channel.

The aforementioned multiple-scales expansion relies on a space-reductive analysis founded on an undetermined scaling transformation (UST). This method of analysis necessitates the introduction of an undetermined scaling variable s that may be left unspecified during the derivation process. At the conclusion of the asymptotic analysis, physical arguments are applied towards the determination of s. The idea is anchored on Prandtl's principle of matching with supplementary expansions (Van Dyke 1975, p. 53). Accordingly, the dominant term in the multiple-scales solution is matched to its counterpart from a WKB expansion. The outcome is helpful in disclosing the inherently nonlinear scaling structure of the problem. It also produces a uniformly valid UST solution that outperforms the basic WKB approximation over a range of physical parameters.

Despite the useful feature of retaining an undetermined scale during the derivation process, the UST scheme bears practical limitations. Its feasibility is contingent on the existence of an alternative approximation. To overcome this deficiency, the present study will extend the UST analysis by presenting a simpler approach which leads to the independent specification of the scaling transformation. This will be obtained by imposing the problem's solvability condition to the extent of suppressing singularity in successive asymptotic orders. We refer to the resulting expansion as GST (generalized scaling technique). This approach is also applied by Majdalani & Rienstra (2002) to problems that involve overlapping dissipative and dispersive

mechanisms. In comparison to the UST expansion, the paradigm to be implemented precludes matching and guesswork.

In connection with the WKB expansions of this problem, our study will discuss the recurrence of an endpoint singularity that only appears at higher orders. To better understand the spurious nature of this anomaly, a WKB approximation is presented to an arbitrary order. In the process, two types of physical solutions are realized. From the expression of type I, a singularity that appears at alternating orders of the perturbation parameter is identified. This singularity will be shown to affect a thin region near the core of the porous channel where the WKB approximation deteriorates. In revisiting this problem, a new solution of type II will be identified and shown to be unconditionally valid to any order.

The paper is arranged into seven sections. In § 2, the problem is briefly defined using the momentum transport formulation. This is followed in § 3 by the formal procedural steps leading to a multi-order WKB expansion. In the course of this effort, the presence of singularities at alternating orders is identified and discussed. In § 4, illustrative examples are provided and the existence of an end-zone boundary layer is ascertained. Section 5 describes the construction of a multiple-scales solution based on a generalized coordinate. Imposition of the problem's solvability condition is then used to deduce the scale. In this manner, a multiple-scales solution is obtained for an arbitrary mean-flow function. In § 6, the axially travelling wave is completed and verified numerically. Its main characteristics are explored and discussed. Finally, main conclusions are reviewed in § 7.

2. Mathematical model

Our main focus is placed on the velocity of a damped travelling wave inside a long porous channel. Based on two previous studies (Majdalani & Van Moorhem 1998; Majdalani 2001), the longitudinal component of the wave can be written as

$$u_1(x,y,t) = \mathrm{i}\,\sin(\omega_m x)\exp(-\mathrm{i}\omega_m t) - \mathrm{i}\sum_{n=0}^{\infty}\frac{(-1)^n(\omega_m x)^{2n+1}}{(2n+1)!}Y_n(y)\exp(-\mathrm{i}\omega_m t)+O(\varepsilon),\quad \begin{cases}0\leqslant x\leqslant l\\ 0\leqslant y\leqslant 1\end{cases} \tag{2.1}$$

where the eigenfunction Y_n must be determined from the doubly perturbed problem connected with

$$\varepsilon\frac{\mathrm{d}^2Y_n}{\mathrm{d}y^2}-\sigma F(y)\frac{\mathrm{d}Y_n}{\mathrm{d}y}+\left[\mathrm{i}+2\sigma(n+1)F'(y)\right]Y_n=0,\ \ 0\leqslant y\leqslant 1,\ \ Y_n(0)=1,\ \ Y_n'(1)=0, \tag{2.2}$$

where

$$\varepsilon=\nu\omega^{-1}h^{-2}\in[10^{-8},10^{-4}]\quad \sigma\equiv S^{-1}=v_w\omega^{-1}h^{-1}\in[10^{-4},10^{-1}]. \tag{2.3}$$

For the reader interested in the steps leading to (2.2), a brief overview is provided in Appendix A. Note that S is the Strouhal number while ε represents the reciprocal of the kinetic Reynolds number. For consistency, we adopt the same notation as before (Majdalani 2001). We use t to denote dimensionless time and x and y to represent the streamwise and transverse coordinates (normalized by the channel's half-spacing h). With v_w as the injection speed at the wall and ν as the kinematic viscosity, we denote the speed of sound by a_s and use asterisks to designate dimensional variables.

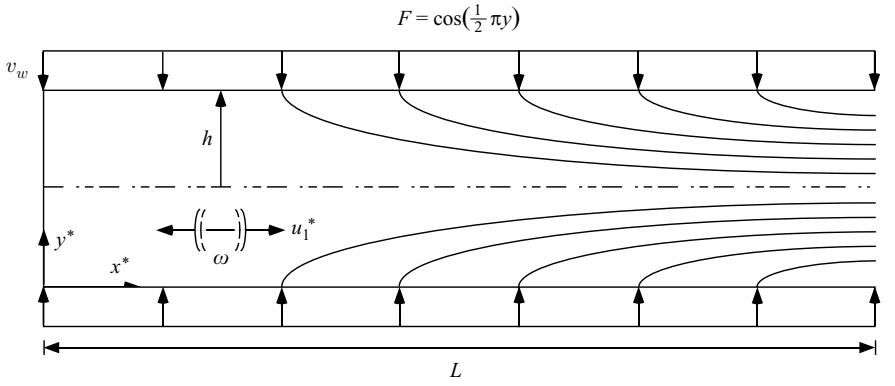

FIGURE 1. Coordinate system and geometric parameters defining the porous channel with sidewall injection.

Our normalization is based on

$$x = x^*/h, \quad y = y^*/h, \quad t = t^* a_s/h,$$
$$\omega_m = \omega h/a_s = m\pi h/L, \quad l = L/h, \quad u_1 = u_1^*/(\bar{\varepsilon} a_s). \quad (2.4)$$

In the foregoing expressions, ω is the frequency of oscillations and $m \in \mathbb{N}^*$ is the acoustic oscillation mode number of a pressure wave of amplitude A inside a channel of length L and mean pressure p_s (see figure 1). The dimensionless wave parameter in (2.4) is given by $\bar{\varepsilon} = A/(\gamma p_s)$ and the injection Mach number by $M_w = v_w/a_s$. With this nomenclature at hand, the instantaneous velocity in the channel becomes

$$\boldsymbol{u}(x, y, t) = M_w \boldsymbol{u}_0(x, y) + \bar{\varepsilon} \boldsymbol{u}_1(x, y, t); \quad \begin{cases} \boldsymbol{u}_0(x, y) = (-xF'(y), F(y)) \\ \boldsymbol{u}_1(x, y, t) = (u_1(x, y, t), O(M_w)) \end{cases}. \quad (2.5)$$

At this juncture, it may be helpful to introduce the injection (or crossflow) Reynolds number as $R \equiv v_w h/\nu = (\varepsilon S)^{-1} > 10$. Then, depending on the value of R, two mean-flow solutions have been made available by Berman (1953) and Yuan (1956). These correspond to

$$F(y) = \begin{cases} 1 - \frac{3}{2}y^2 + \frac{1}{2}y^3, & 10 < R < 100 \\ \cos\theta, \theta \equiv \frac{1}{2}\pi y, & R > 100 \end{cases}, \quad \text{where} \begin{cases} F'(0) = F(1) = F''(1) = 0 \\ F(0) \equiv F_0 = 1 \end{cases}. \quad (2.6)$$

At this point, it is expedient to define the small perturbation parameter $\delta \equiv R^{-1} = \varepsilon S$. In lieu of ε, $\delta < 0.1$ is the principal perturbation parameter used in mean-flow studies of porous channels (Berman 1953, 1958); δ is proportional to the viscosity independently of the oscillation frequency. This viscous parameter is present implicitly in (2.2). It can be displayed by multiplying (2.2) with the Strouhal number to obtain

$$\delta \frac{\mathrm{d}^2 Y_n}{\mathrm{d}y^2} - F\frac{\mathrm{d}Y_n}{\mathrm{d}y} + \left[\mathrm{i}S + 2(n+1)F'\right] Y_n = 0, \quad 0 \leqslant y \leqslant 1, \quad Y_n(0) = 1, \quad Y_n'(1) = 0. \quad (2.7)$$

3. WKB analysis

3.1. *Exponential corrections*

A regular WKB expansion begins with

$$Y_n(y) = \exp\left(\beta^{-1}z_0 + z_1 + \beta z_2 + \beta^2 z_3 + \beta^3 z_4 + \cdots\right), \tag{3.1}$$

where $z_k(y)$ must be determined sequentially for $k \geqslant 0$. Differentiating twice and substituting into (2.2) yields

$$\begin{aligned}\varepsilon\left[\beta^{-2}z_0'^2 + \beta^{-1}(z_0'' + 2z_0'z_1') + z_1'' + z_1'^2 + 2z_0'z_2' + \beta(z_2'' + 2z_0'z_3' + 2z_1'z_2') + \cdots\right]\\ - \sigma F\left(\beta^{-1}z_0' + z_1' + \beta z_2' + \beta^2 z_3' + \beta^3 z_4' + \cdots\right) + \left[\mathrm{i} + 2\,(n+1)\,\sigma F'\right] = 0.\end{aligned} \tag{3.2}$$

In order to distinguish terms of the same order, it is convenient to multiply through by βS so one can write

$$\begin{aligned}\left(\mathrm{i}\beta S - Fz_0'\right) + \beta\left[\delta\beta^{-2}z_0'^2 + 2\,(n+1)\,F' - Fz_1'\right] + \beta^2\left[\delta\beta^{-2}(z_0'' + 2z_0'z_1') - Fz_2'\right]\\ + \beta^3\left[\delta\beta^{-2}(z_1'' + z_1'^2 + 2z_0'z_2') - Fz_3'\right] + O(\beta^4, \delta\beta^2) \equiv 0.\end{aligned} \tag{3.3}$$

3.2. *Main distinguished limits*

Several distinguished limits are possible depending on the relative size of δ and S. For $\delta < S^{-1}$, quantities between brackets will be balanced when $\delta\beta^{-2} = O(1)$ and $\beta S = O(1)$. These conditions are satisfied when $\beta \sim \sqrt{\delta} \sim S^{-1}$ or $\delta \sim S^{-2}$. Since $\xi = \delta S^2 = O(1)$ is indeed a physical characteristic of the problem, a distinguished limit can be established by choosing $\beta \equiv \sqrt{\varepsilon S} = \sqrt{\delta}$. The balanced series in (3.3) becomes

$$\begin{aligned}(\mathrm{i}S\sqrt{\delta} - Fz_0') + \sqrt{\delta}\left[z_0'^2 + 2(n+1)F' - Fz_1'\right] + \delta[(z_0'' + 2z_0'z_1') - Fz_2']\\ + \delta\sqrt{\delta}\left[\left(z_1'' + z_1'^2 + 2z_0'z_2'\right) - Fz_3'\right] + O(\delta^2) \equiv 0.\end{aligned} \tag{3.4}$$

For $\delta \sim S^{-1}$, it can be seen from (3.2) that the distinguished limit must be $\beta \equiv \delta$. Recalling that $\varepsilon = \delta/S$, one can multiply (3.2) by $S\delta$ and write

$$\begin{aligned}z_0'^2 + \delta(z_0'' + 2z_0'z_1') + \delta^2\left(z_1'' + z_1'^2 + 2z_0'z_2'\right) + \delta^3(z_2'' + 2z_0'z_3' + 2z_1'z_2')\\ - F\left(z_0' + \delta z_1' + \delta^2 z_2' + \delta^3 z_3'\right) + \left[\mathrm{i}S + 2\,(n+1)\,F'\right]\delta + O(\delta^4) = 0.\end{aligned} \tag{3.5}$$

A simple rearrangement yields the progressively diminishing series

$$\begin{aligned}\left(z_0'^2 - Fz_0' + \mathrm{i}S\delta\right) + \delta\left[(z_0'' + 2z_0'z_1') - Fz_1' + 2(n+1)F'\right] + \delta^2\left(z_1'' + z_1'^2 + 2z_0'z_2' - Fz_2'\right)\\ + \delta^3(z_2'' + 2z_0'z_3' + 2z_1'z_2' - Fz_3') + O(\delta^4) \equiv 0.\end{aligned} \tag{3.6}$$

3.3. *The WKB solution of type I*

For $\beta = \sqrt{\delta}$, $\delta \sim S^{-2}$, terms of like power in δ can be collected. The dominant part in (3.4), namely, $-Fz_0' + \mathrm{i}S\sqrt{\delta} = 0$, $z_0(0) = 0$, can be readily integrated into

$$z_0(y) = \mathrm{i}S\sqrt{\delta}\int_0^y F^{-1}(z)\,\mathrm{d}z. \tag{3.7}$$

Similarly, the $O(1)$ equation, $-Fz_1' + z_0'^2 + 2(1+n)F' = 0,\ z_1(0) = 0$, leads to

$$z_1(y) = -\xi \int_0^y F^{-3}(z)\,\mathrm{d}z + 2(1+n)\ln(F/F_0); \quad \xi = \delta S^2. \tag{3.8}$$

Next, $-Fz_2' + z_0'' + 2z_0'z_1' = 0$ can be integrated with $z_2(0) = 0$. One finds

$$z_2(y) = \int_0^y F^{-1}\left(z_0'' + 2z_0'z_1'\right)\mathrm{d}z = \mathrm{i}S\sqrt{\delta}\left\{-2\xi\int_0^y F^{-5}(z)\,\mathrm{d}z + \left(2n+\tfrac{3}{2}\right)\left[F_0^{-2} - F^{-2}(y)\right]\right\}. \tag{3.9}$$

By substituting (3.7)–(3.9) back into (3.1) and using W for WKB, one obtains the complete zeroth-order solution in δ. This is

$$Y_n^{(0)}(y) = (F/F_0)^{2n+2}\exp\left(\zeta_0^W - \mathrm{i}\Phi_0^W - \mathrm{i}\Phi_{1n}^W\right) + O(\delta), \tag{3.10}$$

where

$$\zeta_0^W = -\xi\int_0^y F^{-3}\,\mathrm{d}z, \quad \Phi_0^W = -S\int_0^y F^{-1}\,\mathrm{d}z,$$
$$\Phi_{1n}^W = \delta S\left\{2\xi\int_0^y F^{-5}(z)\,\mathrm{d}z + \left(2n+\tfrac{3}{2}\right)\left[F^{-2}(y) - F_0^{-2}\right]\right\}. \tag{3.11}$$

Equation (3.10) defines the basic WKB solution. This expression constitutes an improvement over the $O(\delta S)$ solution reported by Majdalani (2001). The inclusion of Φ_{1n}^W is necessary to complete the leading-order WKB expression.

Higher order solutions may be generated recursively. However, two successive corrections in z_k are needed to advance, at each level, by one order in δ. For example, z_3 and z_4 can be evaluated from

$$z_3 = \int_0^y F^{-1}\left(z_1'^2 + z_1'' + 2z_0'z_2'\right)\mathrm{d}z = 2(n+1)\left[F'F^{-2} + (2n+3)\int_0^y F'^2F^{-3}\,\mathrm{d}z\right]$$
$$+ \tfrac{1}{4}\xi(12n+7)\left(F^{-4} - F_0^{-4}\right) + 5\xi^2\int_0^y F^{-7}\,\mathrm{d}z, \tag{3.12}$$

$$z_4 = \int_0^y F^{-1}\left(z_2'' + 2z_0'z_3' + 2z_1'z_2'\right)\mathrm{d}z = \mathrm{i}S\sqrt{\delta}\left\{(8n+7)F'F^{-4} + (24n^2+60n+35)\right.$$
$$\left.\times\int_0^y F'^2F^{-5}\,\mathrm{d}z + \tfrac{1}{3}(20n+9)\xi\left(F^{-6} - F_0^{-6}\right) + 14\xi^2\int_0^y F^{-9}\,\mathrm{d}z\right\}. \tag{3.13}$$

The corresponding corrections (i.e. $\zeta_{1n}^W = \delta z_3$ and $\Phi_{2n}^W = \mathrm{i}\delta^{3/2}z_4$) involve higher order integrals; nonetheless, they may be added to the real and imaginary arguments in (3.10) to arrive at a solution of $O(\delta^2)$. Using the solution order as a superscript, it can be seen from (3.1) that

$$Y_n^{(0)} = (F/F_0)^{2n+2}\exp\left(\zeta_0^W - \mathrm{i}\Phi_0^W - \mathrm{i}\Phi_{1n}^W\right) + O(\delta), \tag{3.14}$$

$$Y_n^{(1)} = (F/F_0)^{2n+2}\exp\left(\zeta_0^W + \zeta_{1n}^W - \mathrm{i}\Phi_0^W - \mathrm{i}\Phi_{1n}^W - \mathrm{i}\Phi_{2n}^W\right) + O(\delta^2), \tag{3.15}$$

so that, for $j \geqslant 0$,

$$Y_n^{(j)} = (F/F_0)^{2n+2}\exp\left(\sum_{k=0}^{j}\zeta_{kn}^W - \mathrm{i}\sum_{k=0}^{j+1}\Phi_{kn}^W\right) + O(\delta^{j+1}), \tag{3.16}$$

where $\zeta_{kn}^{W} = \delta^{k} z_{2k+1}$ and $\Phi_{kn}^{W} = \mathrm{i}\delta^{k-1/2} z_{2k}$. Higher order corrections may be derived from

$$z_5 = \int_0^y F^{-1}\left(z_2'^2 + z_3'' + 2z_0'z_4' + 2z_1'z_3'\right) \mathrm{d}z,$$

$$z_6 = \int_0^y F^{-1}\left(z_4'' + 2z_0'z_5' + 2z_1'z_4' + 2z_2'z_3'\right) \mathrm{d}z, \text{ etc.} \quad (3.17)$$

Based on z_0 and z_1, recurring trends may be carefully examined to deduce

$$z_{k+2} = \int_0^y F^{-1} \left\{ \tfrac{1}{2}\left[1-(-1)^k\right] z_{\frac{1}{2}(k+1)}'^2 + z_k'' + 2\sum_{i=0}^{\frac{1}{2}k} z_i' z_{k-i+1}' \right\} \mathrm{d}z; \quad k \in \mathbb{N}. \quad (3.18)$$

When substituted back into (3.1), (3.18) leads to $Y_n^{(j)} = \exp[\delta^{-\frac{1}{2}} z_0 + z_1 + \sum_{k=0}^{2j} \delta^{\frac{1}{2}(k+1)} z_{k+2}] + O(\delta^{j+1})$. Finally, after some effort, we obtain the jth order WKB solution of type I, specifically

$$Y_n^{(j)} = (F/F_0)^{2n+2} \exp\left[-\xi \int_0^y F^{-3}\, \mathrm{d}z + \mathrm{i}S \int_0^y F^{-1}\, \mathrm{d}z + \sum_{k=0}^{2j} \delta^{\frac{1}{2}(k+1)} z_{k+2}\right]$$

$$+ O(\delta^{j+1}) = \left(\frac{F}{F_0}\right)^{2n+2} \exp\left[\int_0^y F^{-1}\left(-\xi F^{-2} + \mathrm{i}S + \sum_{k=0}^{2j} \delta^{\frac{1}{2}(k+1)}\right.\right.$$

$$\left.\left. \times \left\{ \tfrac{1}{2}[1-(-1)^k] z_{\frac{1}{2}(k+1)}'^2 + z_k'' + 2\sum_{i=0}^{\frac{1}{2}k} z_i' z_{k-i+1}' \right\}\right) \mathrm{d}z\right] + O(\delta^{j+1}). \quad (3.19)$$

From the WKB solution of type I, it can be shown that for odd values of j, a singularity arises as $y \to 1^-$, $\forall n$. The non-uniformity near the core can be attributed to the appearance of a shear layer that arises when small exponential corrections in even powers of δ are retained. The presence of a boundary layer near the core is consistent with the classic theory of laminar, injection-driven flows (Terrill 1965, 1973).

3.4. *The WKB solution of type II*

For $\beta = \delta$, $\delta \sim S^{-1}$, terms of integral powers in δ may be segregated. The eikonal equation in (3.6), namely, $z_0'^2 - Fz_0' + \mathrm{i}S\delta = 0$, $z_0(0) = 0$, yields two possible solutions. These correspond to

$$z_0(y) = \tfrac{1}{2} \int_0^y \left[F(z) \mp \sqrt{F^2(z) - 4\mathrm{i}S\delta}\right] \mathrm{d}z. \quad (3.20)$$

In turn, the transport equation, $(z_0'' + 2z_0'z_1') - Fz_1' + 2(n+1)F' = 0$, $z_1(0) = 0$, can be managed in closed form. Integration requires the use of $\int (F'/\sqrt{F^2 - 4\mathrm{i}S\delta})\, \mathrm{d}z =$

$\ln\,[F(z)+\sqrt{F^2(z)-4\mathrm{i}S\delta}]+c$ and leads to the dual solutions:

$$z_1(y)=\int_0^y \frac{z_0''+2(n+1)F'}{F-2z_0'}\,\mathrm{d}z=\ln\left\{\left[\frac{F_0^2-4\mathrm{i}S\delta}{F^2(y)-4\mathrm{i}S\delta}\right]^{\frac{1}{4}}\times\left[\frac{F(y)+\sqrt{F^2(y)-4\mathrm{i}S\delta}}{F_0+\sqrt{F_0^2-4\mathrm{i}S\delta}}\right]^{\pm\left(2n+\frac{5}{2}\right)}\right\}. \quad (3.21)$$

Using K_n to denote the WKB solution of type II, the linearity of (2.2) enables us to put, at $O(\delta)$,

$$K_n=C_1\left[\frac{F_0^2-4\mathrm{i}S\delta}{F^2(y)-4\mathrm{i}S\delta}\right]^{\frac{1}{4}}\left[\frac{F(y)+\sqrt{F^2(y)-4\mathrm{i}S\delta}}{F_0+\sqrt{F_0^2-4\mathrm{i}S\delta}}\right]^{2n+\frac{5}{2}}\exp\left\{\tfrac{1}{2}\delta^{-1}\int_0^y[F(z)-\sqrt{F^2(z)-4\mathrm{i}S\delta}]\,\mathrm{d}z\right\}+C_2\left[\frac{F_0^2-4\mathrm{i}S\delta}{F^2(y)-4\mathrm{i}S\delta}\right]^{\frac{1}{4}}\left[\frac{F(y)+\sqrt{F^2(y)-4\mathrm{i}S\delta}}{F_0+\sqrt{F_0^2-4\mathrm{i}S\delta}}\right]^{-2n-\frac{5}{2}}\times\exp\left\{\tfrac{1}{2}\delta^{-1}\int_0^y[F(z)+\sqrt{F^2(z)-4\mathrm{i}S\delta}]\,\mathrm{d}z\right\}. \quad (3.22)$$

At this juncture, the two constants $C_1=1$ and $C_2=0$ are determined such that the two boundary conditions, $K_n(0)=1$ and $K_n'(1)=0$ are secured. The result is

$$Y_n^K\equiv K_n^{(0)}=\left[\frac{F_0^2-4\mathrm{i}S\delta}{F^2(y)-4\mathrm{i}S\delta}\right]^{\frac{1}{4}}\left[\frac{F(y)+\sqrt{F^2(y)-4\mathrm{i}S\delta}}{F_0+\sqrt{F_0^2-4\mathrm{i}S\delta}}\right]^{2n+\frac{5}{2}}\times\exp\left\{\tfrac{1}{2}\delta^{-1}\int_0^y[F(z)-\sqrt{F^2(z)-4\mathrm{i}S\delta}]\,\mathrm{d}z\right\}. \quad (3.23)$$

Recalling from (2.6) that $F_0=1$ and $F(1)=0$, (3.23) may be evaluated at the core. One finds

$$Y_n^K(1)=\delta^{n+1}\left(\sqrt{1-4\mathrm{i}S\delta}\right)^{\frac{1}{2}}(1+\sqrt{1-4\mathrm{i}S\delta})^{-2n-\frac{5}{2}}(-4\mathrm{i}S)^{n+1}\times\exp\left\{\tfrac{1}{2}\delta^{-1}\int_0^1(F-\sqrt{F^2-4\mathrm{i}S\delta})\mathrm{d}z\right\}\sim O(\delta^{n+1}). \quad (3.24)$$

Further corrections can be systematically unravelled. From $z_1''+z_1'^2+2z_0'z_2'-Fz_2'=0$, one gets

$$z_2=\int_0^y (z_1''+z_1^2)/(F-2z_0')\,\mathrm{d}z. \quad (3.25)$$

Similarly, the $O(\delta^3)$ equation $z_2''+2z_0'z_3'+2z_1'z_2'-Fz_3'=0$ gives $z_3=\int_0^y[(z_2''+2z_1'z_2')/(F-2z_0')]\,\mathrm{d}z$. A recurrence formula is identified for $k\geqslant 0$ such that

$$z_{k+3}=\int_0^y\left[\left(z_{k+2}''+2z_1'z_{k+2}'+\sum_{i=1}^{k}z_{i+1}'z_{k+2-i}'\right)\Big/(F-2z_0')\right]\mathrm{d}z. \quad (3.26)$$

This expression enables us to write, for $j \geqslant 2$,

$$K_n^{(j)} = \exp\left(\delta^{-1}z_0 + z_1 + \delta z_2 + \sum_{k=0}^{j-2}\delta^{k+2}z_{k+3}\right) + O(\delta^{j+1})$$
$$= K_n^{(0)}\exp\int_0^y \left\{(F-2z_0')^{-1}\left[\delta\left(z_1'' + z_1^2\right) + \sum_{k=0}^{j-2}\delta^{k+2}\left(z_{k+2}'' + 2z_1'z_{k+2}' + \sum_{i=1}^{k} z_{i+1}'z_{k+2-i}'\right)\right]\mathrm{d}z\right\} + O(\delta^{j+1}). \tag{3.27}$$

3.5. *Other possible limits*

For $\beta = \delta^{1/3},\ \delta \sim S^{-3}$, a type III expansion may also be conceived. As usual, terms of equal powers in δ may be combined and the leading-order terms that emerge in (3.3), namely, $z_0' - \mathrm{i}S\delta^{1/3}F^{-1} = 0$ with $z_0(0) = 0$, can be integrated. One gets

$$z_0(y) = \mathrm{i}S\delta^{1/3}\int_0^y F^{-1}(z)\,\mathrm{d}z. \tag{3.28}$$

In like fashion, one extracts, $z_1' = 2(n+1)F^{-1}F',\ z_2' = F^{-1}z_0'^2,\ z_1(0) = z_2(0) = 0$ and so on. These first-order ordinary differential equations (ODEs) yield

$$z_1(y) = 2(n+1)\ln(F/F_0); z_2(y) = -S^2\delta^{2/3}\int_0^y F^{-3}(z)\,\mathrm{d}z, \tag{3.29}$$

$$z_3 = \int_0^y F^{-1}(2z_0'z_1' + z_0'')\,\mathrm{d}z = \mathrm{i}S\delta^{1/3}\left(2n + \tfrac{3}{2}\right)\left(F_0^{-2} - F^{-2}\right). \tag{3.30}$$

Starting at z_3, the type III formulation is seen reproduce the type I solution obtained at a previous order. As before, a recursive formula may be identified for $k \geqslant 0$, specifically

$$z_{k+3} = \int_0^y F^{-1}\left\{\tfrac{1}{2}[1-(-1)^k]z'^2_{\frac{1}{2}(k+1)} + z_k'' + 2\sum_{i=0}^{\frac{1}{2}k} z_i'z_{k-i+1}'\right\}\mathrm{d}z;\ \ k \in \mathbb{N}. \tag{3.31}$$

Thus, for $j \geqslant 2$, one is left with

$$B_n^{(j)} = (F/F_0)^{2n+2}\exp\left(\mathrm{i}S\int_0^y F^{-1}(z)\,\mathrm{d}z - \xi\int_0^y F^{-3}(z)\,\mathrm{d}z + \sum_{k=0}^{j-2}\delta^{\frac{1}{3}(k+2)}z_{k+3}\right) + O(\delta^{j+1})$$
$$= \left(\frac{F}{F_0}\right)^{2n+2}\exp\left[\int_0^y F^{-1}\left(-\xi F^{-2} + \mathrm{i}S + \sum_{k=0}^{j-2}\delta^{\frac{1}{3}(k+2)}\right.\right.$$
$$\left.\left.\times\left\{\tfrac{1}{2}[1-(-1)^k]z'^2_{\frac{1}{2}(k+1)} + z_k'' + 2\sum_{i=0}^{\frac{1}{2}k} z'_i z'_{k-i+1}\right\}\right)\mathrm{d}z\right] + O(\delta^{j+1}), \tag{3.32}$$

where $B_n^{(j)}$ refers to the WKB approximation of type III. Interestingly, it may be shown that $B_n^{(j)}$ reproduces $Y_n^{(j)}$ when truncated at the same order in δ. This trend extends to other types of expansions that may be obtained using distinguished limits

corresponding to $\delta \sim S^{-4},\ S^{-5},\ S^{-6}$, etc. These appear to represent slower converging series of type I that share similar physical attributes. For this reason, only the type I expansion will be considered in the remainder of this study.

3.6. *The total velocity field*

To express the time-dependent axial velocity, one substitutes the eigenfunctions into (2.1). Based on the WKB solution of type I, one obtains

$$u_1^W(x, y, t) = \mathrm{i}\,\sin(\omega_m x)\exp(-\mathrm{i}\omega_m t) - \mathrm{i}(F/F_0)\,\sin(\omega_m x F/F_0)\exp\left[\zeta^W - \mathrm{i}\left(\omega_m t + \Phi^W\right)\right] + O(\delta). \quad (3.33)$$

The real part may be readily retrieved and written as

$$u_1^W(x, y, t) = \sin(\omega_m x)\,\sin(\omega_m t) - (F/F_0)\,\sin(\omega_m x F/F_0)\exp\zeta^W \sin\left(\omega_m t + \Phi^W\right) + O(\delta). \quad (3.34)$$

As for the arguments in (3.34), they can be determined from the known functions

$$\zeta^W = -\delta S^2 \int_0^y F^{-3}(z)\,\mathrm{d}z,\ \Phi^W = -S\int_0^y F^{-1}(z)\,dz - \delta S\left[\tfrac{3}{2}\left(F_0^{-2} - F^{-2}\right) - 2\delta S^2 \int_0^y F^{-5}(z)\,\mathrm{d}z\right]. \quad (3.35)$$

Attempts to express (3.34) at orders higher than $\delta \sim S^{-2}$ are needless because u_1 is derived from the momentum equation at the order of S^{-2}. This constitutes another justification for dismissing asymptotic expansions that occur at $\delta \sim S^{-k}$; $k \geqslant 3$.

Based on the WKB solution of type II, one can start with

$$u_1^K(x, y, t) = \mathrm{i}\,\sin(\omega_m x)\exp(-\mathrm{i}\omega_m t) - \mathrm{i}\sum_{n=0}^{\infty} \frac{(-1)^n\,(\omega_m x)^{2n+1}}{(2n+1)!} K_n(y)\exp(-\mathrm{i}\omega_m t) + O(\delta) \quad (3.36)$$

and then insert (3.23). One finds

$$u_1^K(x, y, t) = \mathrm{i}\,\sin(\omega_m x)\exp(-\mathrm{i}\omega_m t) - \mathrm{i} \times \exp(-\mathrm{i}\omega_m t)\exp\left\{\tfrac{1}{2}\delta^{-1}\int_0^y \left[F(z) - \sqrt{F^2(z) - 4\mathrm{i}S\delta}\right]\mathrm{d}z\right\} \times \left(\frac{F_0^2 - 4\mathrm{i}S\delta}{F^2 - 4\mathrm{i}S\delta}\right)^{\frac{1}{4}} \left(\frac{F + \sqrt{F^2 - 4\mathrm{i}S\delta}}{F_0 + \sqrt{F_0^2 - 4\mathrm{i}S\delta}}\right)^{\frac{3}{2}} \times \sum_{n=0}^{\infty} \frac{(-1)^n\,(\omega_m x)^{2n+1}}{(2n+1)!} \left(\frac{F + \sqrt{F^2 - 4\mathrm{i}S\delta}}{F_0 + \sqrt{F_0^2 - 4\mathrm{i}S\delta}}\right)^{2n+1} + O(\delta). \quad (3.37)$$

At this juncture, the MacLaurin series expansion of the sine function can be identified in (3.37). This enables us to simplify (3.37) into

$$u_1^K(x, y, t) = \mathrm{i}\,\sin(\omega_m x)\exp(-\mathrm{i}\omega_m t) - \mathrm{i}\exp(-\mathrm{i}\omega_m t) \times \exp\left\{\tfrac{1}{2}\delta^{-1}\int_0^y \left[F(z) - \sqrt{F^2(z) - 4\mathrm{i}S\delta}\right]\mathrm{d}z\right\}$$

$$\times \left(\frac{F_0^2 - 4\mathrm{i}S\delta}{F^2 - 4\mathrm{i}S\delta}\right)^{\frac{1}{4}} \left(\frac{F + \sqrt{F^2 - 4\mathrm{i}S\delta}}{F_0 + \sqrt{F_0^2 - 4\mathrm{i}S\delta}}\right)^{\frac{3}{2}}$$

$$\times \sin[\omega_m x(F + \sqrt{F^2 - 4\mathrm{i}S\delta})/(F_0 + \sqrt{F_0^2 - 4\mathrm{i}S\delta})] + O(\delta). \quad (3.38)$$

A closed form type II solution depends on the tacit integration of the exponential argument in (3.38). Despite its accuracy and well-behaved character, the radical in the integrand of u_1^K makes it less susceptible to integration. Hence, in cases for which numerical evaluation is unavoidable, the type I u_1^W becomes more practical.

4. Illustrative examples

Two applications to porous channels may be considered for which $F = 1 - \frac{3}{2}y^2 + \frac{1}{2}y^3$ when $10 < R < 100$ and $F = \cos(\frac{1}{2}\pi y)$ when $R \to \infty$. Moreover, the test case for $F = \alpha(1 - y)$ will be investigated as it represents a generic function that can effectively mimic the asymptotic behaviour of the solution near the core.

4.1. *Asymptotic solutions for small and large R*

For small and large R, the type I solution $Y_n^{(0)}$may be determined directly from

$$\int_0^y F^{-1}(z)\,\mathrm{d}z = \begin{cases} \frac{1}{3}\ln\left[\left(1 + y - \frac{1}{2}y^2\right)(1 - y)^2\right], & \text{small } R \\ \frac{2}{\pi}\ln\tan\left[\frac{\pi}{4}(1 + y)\right], & \text{large } R \end{cases}, \quad (4.1)$$

$$\int_0^y F^{-3}(z)\,\mathrm{d}z = \begin{cases} \frac{4}{27}\ln\frac{3-r^2}{2r^2} + \frac{4r^4 - 18r^2 + 12}{9r^2(3-r^2)^2} + \frac{1}{18}, & \text{small } R \\ \frac{1}{\pi}\left[\ln\tan\frac{1}{4}\pi(1 + y) + \sec\left(\frac{1}{2}\pi y\right)\tan\left(\frac{1}{2}\pi y\right)\right], & \text{large } R \end{cases}, \quad (4.2)$$

where $r \equiv 1 - y$ and

$$\int_0^y F^{-5}(z)\,\mathrm{d}z$$

$$= \begin{cases} \frac{4}{729}\left\{\frac{147}{16} + 20\ln(-\frac{1}{2} + \frac{3}{2}r^{-2}) + 3[2 + y^2(y-3)]^{-4}\left[-49 + y(y-2)(-326\right.\right. \\ \left.\left. + 5y(y-2)\ \{31 + 2y(y-2)[-2 + y(y-2)]\,[-7 + 2y(y-2)]\}\right)\right]\}, & \text{small } R \\ \frac{1}{16\pi}\left\{12\ln\tan\left(\frac{1}{4}\pi + \frac{1}{2}\theta\right) + \sec^4\theta\,[3\sin(3\theta) + 11\sin\theta]\right\}, & \text{large } R \end{cases}. \quad (4.3)$$

Note that for both small and large R, (3.10) gives $Y_0^{(0)}(1) = 0$ at the core. For the type II solution, the leading-order expansion (3.23) may be evaluated for large R to arrive at

$$K_n^{(0)} = \left(\frac{1 - 4\mathrm{i}S\delta}{\cos^2\theta - 4\mathrm{i}S\delta}\right)^{\frac{1}{4}} \left(\frac{\cos\theta + \sqrt{\cos^2\theta - 4\mathrm{i}S\delta}}{1 + \sqrt{1 - 4\mathrm{i}S\delta}}\right)^{2n + \frac{5}{2}}$$

$$\times \exp\left(\tfrac{1}{\pi\delta}\{\sin\theta - \sqrt{1 - 4\mathrm{i}S\delta}E[\theta|(1 - 4\mathrm{i}S\delta)^{-1}]\}\right), \quad (4.4)$$

where $E(\theta|x) = \int_0^\theta \sqrt{1 - x\sin^2 z}\,\mathrm{d}z$ is the elliptic integral of the second kind. At the core, one regains the complete elliptic integral $E(x) \equiv E(\frac{1}{2}\pi|x) =$

	WKB type I			WKB type II			Numerical
y	$Y_0^{(0)}$	$Y_0^{(1)}$	$Y_0^{(2)}$	$K_0^{(0)}$	$K_0^{(1)}$	$K_0^{(2)}$	Y_0^N
0.00	1	1	1	1	1	1	1
0.05	0.8676644	0.8674551	0.8674590	0.8676685	0.8674590	0.8674590	0.8674590
0.10	0.5188763	0.5186301	0.5186429	0.5188833	0.5186428	0.5186429	0.5186429
0.20	−0.3939219	−0.3935576	−0.3935347	−0.3939428	−0.3935340	−0.3935347	−0.3935347
0.30	−0.7672007	−0.7662141	−0.7662170	−0.7672949	−0.7662147	−0.7662170	−0.7662171
0.40	−0.2589166	−0.2585327	−0.2585659	−0.2589812	−0.2585645	−0.2585659	−0.2585659
0.50	0.3586916	0.3582113	0.3582018	0.3589124	0.3581976	0.3582018	0.3582018
0.60	0.2062112	0.2061807	0.2061778	0.2064960	0.2061744	0.2061778	0.2061778
0.70	−0.1574955	−0.1582490	−0.1582805	−0.1582560	−0.1582757	−0.1582805	−0.1582805
0.80	0.0345428	0.0357267	0.0360158	0.0356684	0.0360156	0.0360158	0.0360158
0.90	−0.0049035	−0.0104253	−0.0091613	−0.0088040	−0.0091688	−0.0091612	−0.0091613
0.95	−0.0000306	34513650.	0.0008021	0.0006995	0.0008034	0.0008017	0.0008015
1.00	0	∞	0	−0.0000111	−0.0000168	−0.0000170	−0.0000339

TABLE 1. Comparison between numerical and asymptotic solutions using the two WKB approximations, $Y_n^{(j)}$ and $K_n^{(j)}$, given at $O(\delta^{j+1})$. Here $S = 10$, $R = 10^3$, $n = 0$ and $F = \cos(\frac{1}{2}\pi y)$.

$\pi\left(\frac{1}{2} - \frac{1}{8}x - \frac{3}{128}x^2 - \frac{5}{512}x^3 - \frac{175}{32768}x^4 + \cdots\right)$. Consequently, one may express

$$K_n^{(0)}(1) = \delta^{n+1}(-4\mathrm{i}S)^{n+1}(\sqrt{1-4\mathrm{i}S\delta})^{\frac{1}{2}}(1+\sqrt{1-4\mathrm{i}S\delta})^{-2n-\frac{5}{2}} \times \exp\left(\tfrac{1}{\pi\delta}\{1-\sqrt{1-4\mathrm{i}S\delta}E[(1-4\mathrm{i}S\delta)^{-1}]\}\right). \quad (4.5)$$

Higher order approximations may be sequentially generated. For small R, however, only a quasi-analytical solution is possible due to the inability to integrate the eikonal equation except by computer. This issue is not present in the WKB solution of type I.

For large R, a comparison between numerics and asymptotics is provided in table 1. As usual, the agreement between asymptotics and numerics improves at higher orders. For the type II approximations (second set of columns), it is clear that $K_n^{(j)}$ remains uniformly valid $\forall j$. Furthermore, $K_n^{(j)}$ is seen to predict the $O(\delta^{n+1})$ value obtained numerically at $y = 1$. This result is consistent with (4.5). In contrast, the type I solution is shown to exhibit a region of non-uniformity in the vicinity of $y = 1$. Whereas both $Y_n^{(0)}$ and $Y_n^{(2)}$ vanish at the endpoint, $Y_n^{(1)}$ becomes suddenly unbounded as $y \to 1^-$. This behaviour signals the presence of a boundary layer that is not accounted for in the WKB representation of type I. A solution that incorporates small changes inside this layer is therefore necessary.

4.2. *Exact and asymptotic solutions near the core*

Consider $F = \alpha r$ where $\alpha = (\frac{3}{2}, \frac{1}{2}\pi)$ can mimic the small or large injection flow behaviour near the core. As shown in Appendix B, (2.7) can be solved exactly and put in the form

$$Y_n^E = \exp\left[\tfrac{1}{2}\alpha\delta^{-1}\left(1-r^2\right)\right]\frac{\Phi\left(n+\frac{3}{2}-\frac{1}{2}\mathrm{i}\alpha^{-1}S,\,\frac{1}{2},\,\frac{1}{2}\alpha\delta^{-1}r^2\right)}{\Phi\left(n+\frac{3}{2}-\frac{1}{2}\mathrm{i}\alpha^{-1}S,\,\frac{1}{2},\,\frac{1}{2}\alpha\delta^{-1}\right)}. \quad (4.6)$$

Using the WKB expansion of type I, one can obtain an approximation to any desired order such as

$$Y_n^{(0)} = r^{2n+2-\mathrm{i}S/\alpha} \exp\left\{-\tfrac{1}{2}\alpha^{-3}\delta S^2(r^{-2}-1) \right. \\ \left. -\tfrac{1}{2}\mathrm{i}\alpha^{-2}\delta S(r^{-2}-1)\left[3+4n+\delta S^2\alpha^{-3}(r^{-2}+1)\right]\right\} + O(\delta), \quad (4.7)$$

$$Y_n^{(1)} = Y_n^{(0)} \exp\left(\alpha^{-1}\delta(1+n)(1+2n)(r^{-2}-1)\right. \\ +\tfrac{1}{4}\alpha^{-4}\delta^2 S(r^{-4}-1)\{(7+12n)S+\mathrm{i}\alpha[7+4n(7+6n)]\} \\ \left.+\tfrac{1}{3}\alpha^{-7}\delta^3 S^3(r^{-6}-1)\left[\tfrac{5}{2}S+\mathrm{i}\alpha(9+20n)\right]+\tfrac{7}{4}\mathrm{i}\alpha^{-9}\delta^4 S^5(r^{-8}-1)\right)+O(\delta^2), \quad (4.8)$$

$$Y_n^{(2)} = Y_n^{(1)} \exp\left(-\tfrac{1}{2}\alpha^{-2}\delta^2 S^4(1+n)(1+2n)(1+4n)(r^{-4}-1)-\tfrac{1}{3}\alpha^{-5}\delta^3 S(r^{-6}-1)\right. \\ \times\left\{2[5+3n(9+10n)]S+\tfrac{1}{2}\mathrm{i}\alpha(1+4n)(9+44n+40n^2)\right\}-\tfrac{1}{8}\alpha^{-8}\delta^4 S^3(r^{-8}-1) \\ \times\{(47+140n)S+2\mathrm{i}\alpha[25+4n(47+70n)]\}-\tfrac{1}{5}\alpha^{-11}\delta^5 S^5(r^{-10}-1) \\ \left.\times[21S+\mathrm{i}\alpha(59+252n)]-11\,\mathrm{i}\alpha^{-13}\delta^6 S^7(r^{-12}-1)\right)+O(\delta^3). \quad (4.9)$$

The WKB approximation of type II can also be evaluated for the problem at hand. One obtains the leading-order solution from (3.23). At $O(\delta)$, one finds

$$K_n^{(0)} = \left(\frac{\alpha^2-4\mathrm{i}S\delta}{\alpha^2r^2-4\mathrm{i}S\delta}\right)^{\frac{1}{4}}\left(\frac{\alpha r+\sqrt{\alpha^2r^2-4\mathrm{i}S\delta}}{\alpha+\sqrt{\alpha^2-4\mathrm{i}S\delta}}\right)^{2n+\frac{5}{2}-\mathrm{i}\alpha^{-1}S} \\ \times\exp\left\{\frac{\alpha}{4\delta}\left[1-r^2+r\sqrt{r^2-4\mathrm{i}\frac{S\delta}{\alpha^2}}-\sqrt{1-4\mathrm{i}\frac{S\delta}{\alpha^2}}\right]\right\}. \quad (4.10)$$

In like fashion, one arrives at

$$\frac{K_n^{(1)}}{K_n^{(0)}} = \exp\left\{\frac{-(\frac{5}{2}+2n)\alpha^3(1-r^2)}{(\alpha^2-4\mathrm{i}S\delta)(\alpha^2r^2-4\mathrm{i}S\delta)}+\tfrac{1}{24}\alpha^2(138+240n+96n^2)\right. \\ \times\left[(\alpha^2-4\mathrm{i}S\delta)^{-\frac{3}{2}}-r(\alpha^2r^2-4\mathrm{i}S\delta)^{-\frac{3}{2}}\right]+\tfrac{1}{24}\mathrm{i}\alpha^4S^{-1}\delta^{-1}(37+60n+24n^2) \\ \left.\times\left[(\alpha^2-4\mathrm{i}S\delta)^{-\frac{3}{2}}-r^3(\alpha^2r^2-4\mathrm{i}S\delta)^{-\frac{3}{2}}\right]\right\}+O(\delta^2). \quad (4.11)$$

Higher order terms are preferably derived from (3.27) using symbolic programming.

4.3. *Comparing exact and asymptotic solutions*

The two WKB formulations of increasing orders are compared to the exact solution in table 2 for a typical set of physical parameters. The agreement between exact and asymptotics, often manifested in several decimal places, helps to confirm the accuracy of the foregoing analysis. As alluded to earlier, it can be seen that the WKB solution of type I yields, in an alternating fashion, either zero or infinity at the core. Being inconsistent with the finite value of Y_n^E, this behaviour suggests investigating an inner solution to supplement $Y_n^{(j)}$ near the core. To gain a clearer picture, differences between exact and asymptotic predictions are plotted in figure 2 for $F = \frac{1}{2}\pi(1-y)$ at $n = 0$ and $n = 10$. In figure 2(*a*), it can be seen that the errors associated

https://doi.org/10.1017/S0022112009007939 Published online by Cambridge University Press

	WKB type I			WKB type II			Exact
y	$Y_0^{(0)}$	$Y_0^{(1)}$	$Y_0^{(2)}$	$K_0^{(0)}$	$K_0^{(1)}$	$K_0^{(2)}$	Y_0^E
0.00	1	1	1	1	1	1	1
0.05	−0.0556490	−0.0556491	−0.0556491	−0.0556490	−0.0556491	−0.0556491	−0.0556491
0.10	−0.7894993	−0.7895045	−0.7895045	−0.7894998	−0.7895045	−0.7895045	−0.7895045
0.20	0.4339311	0.4339380	0.4339380	0.4339318	0.4339380	0.4339380	0.4339380
0.30	0.1687017	0.1687069	0.1687069	0.1687024	0.1687069	0.1687069	0.1687069
0.40	−0.2999705	−0.2999864	−0.2999864	−0.2999728	−0.2999864	−0.2999864	−0.2999864
0.50	−0.2399436	−0.2399662	−0.2399662	−0.2399479	−0.2399662	−0.2399662	−0.2399662
0.60	−0.0946533	−0.0946702	−0.0946702	−0.0946577	−0.0946702	−0.0946702	−0.0946702
0.70	0.0647037	0.0647305	0.0647305	0.0647140	0.0647305	0.0647305	0.0647305
0.80	0.0175739	0.0175998	0.0175997	0.0175895	0.0175998	0.0175997	0.0175997
0.90	−0.0019185	−0.0019641	−0.0019629	−0.0019589	−0.0019630	−0.0019630	−0.0019630
0.95	0.0000072	0.0000413	0.0000180	0.0000259	0.0000307	0.0000307	0.0000261
1.00	0	∞	0	-3.10×10^{-15}	-7.35×10^{-15}	-7.36×10^{-15}	-6.62×10^{-15}

TABLE 2. Comparison between exact and asymptotic solutions using the two WKB approximations. Here $S = 50$, $R = 25 \times 10^3$, $n = 0$ and $F = \frac{1}{2}\pi(1 - y)$.

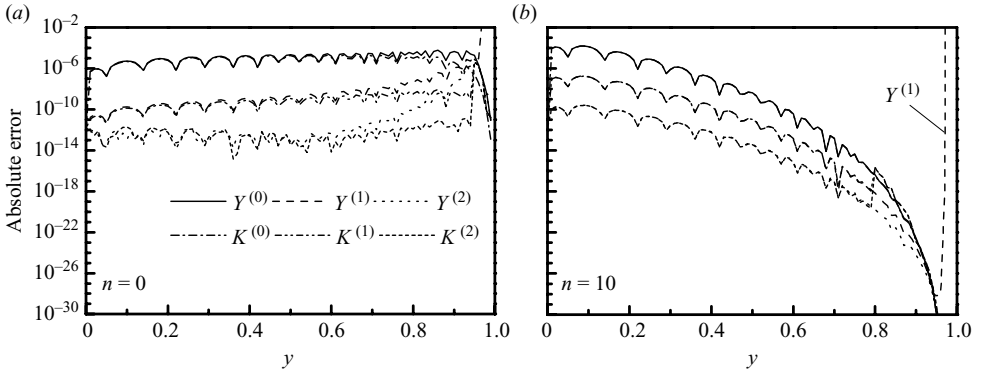

FIGURE 2. Error between exact and asymptotic entries given in table 2 for (*a*) $n = 0$, and (*b*) $n = 10$. Despite its consistent precision in the outer region, $Y^{(1)}$ becomes singular as $y \to 1^-$.

with $Y_n^{(j)}$ and $K_n^{(j)}$ conform to their reported truncation orders, with $K_n^{(j)}$ being somewhat more accurate. Figure 2(*b*), on the other hand, shows that the error in each approximation diminishes as n is increased. It also illustrates the improved agreement between $Y_n^{(j)}$ and $K_n^{(j)}$ at higher values of n. An exception arises in $Y_n^{(1)}$ (odd) which is seen to diverge as $y \to 1^-$. The corresponding region of breakdown is visible in the range $0.96 \leqslant y \leqslant 1$. The core singularity that arises in the WKB solution of type I is difficult to detect because $Y_n^{(1)}$ remains well-behaved and of $O(\delta^2)$ outside the thin region of non-uniformity. This singularity does not affect $K_n^{(j)}, \forall j$.

4.4. *Endpoint singularity at even orders of* $\delta \sim S^{-2}$

It should be noted that as $y \to 1^-$, the WKB solution of type I becomes suddenly unbounded at even orders of δ. This can be explained by considering, for example, the real part of the exponential argument in $Y_n^{(1)}$. This argument controls the wave amplitude and is dominated at the core by $\frac{5}{6}\alpha^{-7}\delta^3 S^4 r^{-6} \xrightarrow[r\to 0^+]{} \infty$ for fixed S, δ and n. Since the wave amplitude is dictated by $r^{2n+2}\exp(\frac{5}{6}\alpha^{-7}\delta^3 S^4 r^{-6})$ as $r \to 0^+$, the exponential singularity cannot be suppressed by the vanishing polynomial. This unbounded character alternates between successive orders in $Y_n^{(j)}$. In fact, as $r \to 0^+$, the amplitude of the WKB solution of type I can be seen to be

$$Y_n^{(0)} \sim r^{2n+2}\exp\left(-\tfrac{1}{2}\alpha^{-3}\delta S^2 r^{-2}\right), Y_n^{(2)} \sim r^{2n+2}\exp\left(-\tfrac{21}{5}\alpha^{-11}\delta^5 S^6 r^{-10}\right), \text{etc.} \tag{4.12}$$

At order j, one finds the key expression

$$Y_n^{(j)} \sim r^{2n+2}\exp\left[\frac{(-1)^{j+1}a_{2j+1}}{(4j+2)\alpha}\frac{\delta^{2j+1}S^{2j+2}}{(\alpha r)^{4j+2}}\right];\ r \to 0^+, \tag{4.13}$$

where $a_0 = a_1 = 1,\ a_2 = 2,\ a_3 = 5,\ a_4 = 14,\ a_5 = 42$, etc. These positive constants form a progressive sequence that can be recovered from

$$a_0 = 1,\quad a_{2j+1} = 2\sum_{k=0}^{j-1} a_k a_{2j-k} + a_j^2,\quad j \geqslant 0;\quad a_{2j} = 2\sum_{k=0}^{j-1} a_k a_{2j-k-1},\quad j \geqslant 1. \tag{4.14}$$

Equation (4.13) exposes an intrinsic singularity at even orders of δ as $r \to 0^+$. For both small and large R, the same type of singularity is detected in the WKB solution of type I. This is caused by the sign alternation of the most singular term following each successive correction to the exponential expansion. Since $Y_n^{(2k+1)}(0)$ becomes unbounded for $k = 0, 1, 2, \ldots$, the use of $Y_n^{(1)}$, $Y_n^{(3)}$, etc., leads to an incomplete

representation. Such a representation lacks exponentially small quantities that arise at even powers of δ. Conversely, since $Y_n^{(2k)}$ satisfies both boundary conditions, it represents an adequate approximation of the exact solution. However, given that $Y_n^{(2k)}(0) = 0$, a problem arises at higher orders because the exact solution does not completely vanish at $r = 0$. To see this, one must evaluate (4.6) viz.

$$Y_n^E(0) = \exp\left(\tfrac{1}{2}\alpha\delta^{-1}\right)/\Phi\left(n + \tfrac{3}{2} - \tfrac{1}{2}\mathrm{i}\alpha^{-1}S,\, \tfrac{1}{2},\, \tfrac{1}{2}\alpha\delta^{-1}\right). \tag{4.15}$$

Then, using the large x identity (Abramowitz & Stegun 1964, p. 504),

$$\Phi(a, b, x) = \frac{\Gamma(b)}{\Gamma(a)} e^x x^{a-b}\left[1 + O(x^{-1})\right], \tag{4.16}$$

one can expand the Kummer function in (4.15) and write

$$Y_n^E(0) = \pi^{-\frac{1}{2}}(2/\alpha)^{1+n-\frac{1}{2}\mathrm{i}\alpha^{-1}S}\Gamma\left(n + \tfrac{3}{2} - \tfrac{1}{2}\mathrm{i}\alpha^{-1}S\right)\delta^{1+n-\frac{1}{2}\mathrm{i}\alpha^{-1}S}\left[1 + O(\delta)\right]. \tag{4.17}$$

Thus, the wave amplitude at the core is seen to be

$$Y_n^E(0) = O(\delta^{1+n}). \tag{4.18}$$

The same can be extrapolated from the WKB solution of type II. In fact, (4.10) gives

$$K_n^{(0)}(0) = \delta^{1+n-\frac{1}{2}\mathrm{i}\alpha^{-1}S}\left(\delta + \tfrac{1}{4}\mathrm{i}\alpha^2 S^{-1}\right)^{\frac{1}{4}}\left[\frac{2(-1)^{\frac{3}{4}}\alpha^{-1}S^{\frac{1}{2}}}{1 + \sqrt{1 - 4\mathrm{i}S\delta\alpha^{-2}}}\right]^{2n+\frac{5}{2}-\mathrm{i}\alpha^{-1}S}$$
$$\times \exp\left[\tfrac{1}{4}\delta^{-1}\alpha(1 - \sqrt{1 - 4\mathrm{i}S\delta\alpha^{-2}})\right] = O(\delta^{1+n}). \tag{4.19}$$

Since the discrepancy between $Y_n^E(0)$ and $Y_n^{(0)}(0)$ is of order $\delta^{1+n} \leqslant \delta$, $\forall n \geqslant 0$, it is generally smaller than the truncation error in the leading-order approximation. It can be safely absorbed by the truncation error. We conclude that $Y_n^{(0)}$ is uniformly valid, $\forall n \geqslant 0$. This behaviour is illustrated in figure 3 where both $Y_0^{(0)}$ and $K_0^{(0)}$ are shown to provide suitable approximations uniformly across the domain. Figure 3 also illustrates the importance of the (viscous) parameter $\xi = \delta S^2$. By fixing ξ, a constant depth of penetration is realized irrespective of the operating parameters. This convincing observation is consistent with the findings of Majdalani (2001). Since the remaining oscillations in the inner region are of $O(\delta)$, their contribution is negligible at leading order. Nonetheless, the discrepancy at the core can become larger than the truncation error in higher order representations. For example, at $O(\delta^3)$, $Y_n^{(2)}$ can become non-uniformly valid for $n = 0, 1$. In general, the discrepancy at the core cannot be ignored in the assessment of $Y_n^{(2k)}$ for $n = 0, 1, \ldots, 2k - 1$; $k \geqslant 1$. Under these auspices, one must insist on an inner correction for $Y_n^{(2k)}$. The removal of the small endpoint discrepancy can be especially useful in applications that demand high precision in the core region. In the oscillatory channel flow problem, the physically meaningful mechanisms occur near the wall where vorticity is generated. Near the core, the rotational coupling with the solid boundary is inconsequential. Although a small exponential correction can be found in the core region, its inclusion is unwarranted at leading order. Beyond the leading order, the type I expansion cannot be continued without displaying a core singularity. When this occurs, an inner correction becomes a necessity.

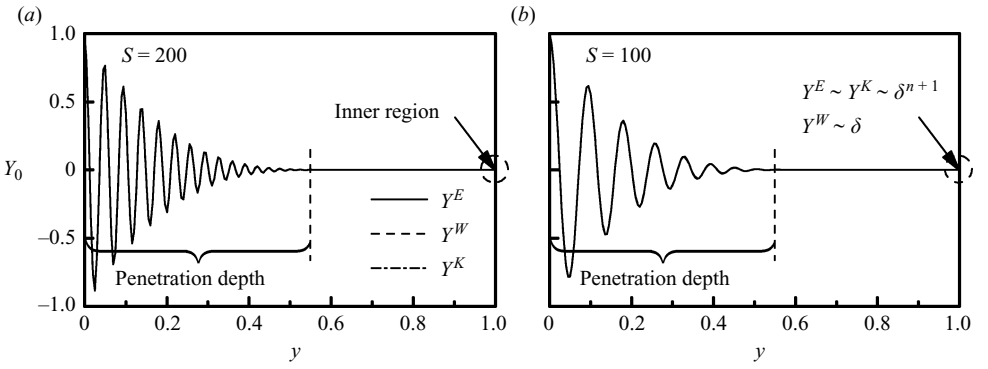

FIGURE 3. WKB approximations showing consistent agreement by overlapping the exact solution for $F = \frac{1}{2}\pi(1-y)$, $\xi = 10$, and a Strouhal number of (*a*) $S = 200$ and (*b*) $S = 100$. By fixing $\xi \equiv \delta S^2$, the penetration depth remains constant irrespective of the frequency of oscillations.

4.5. *The near-core solution*

The inner equation that dominates near the core can be realized following the linear transformation $\chi = r\sqrt{\alpha/\delta}$. One finds

$$\frac{\mathrm{d}^2 Y_n^i}{\mathrm{d}\chi^2} + \chi \frac{\mathrm{d}Y_n^i}{\mathrm{d}\chi} + \left[\mathrm{i}\alpha^{-1}S - (2n+2)\right] Y_n^i = 0, \tag{4.20}$$

where Y_n^i constitutes an inner representation of the solution for $r \in [0, \sqrt{2\delta/\alpha}]$. Equation (4.20) can be readily solved using the boundary condition at the core, $\mathrm{d}Y_n^i(0)/\mathrm{d}\chi = 0$; one obtains

$$Y_n^i(\chi) = C_0\, \mathrm{e}^{-\frac{1}{2}\chi^2} \Phi\left(\tfrac{3}{2} + n - \tfrac{1}{2}\mathrm{i}\alpha^{-1}S,\ \tfrac{1}{2},\ \tfrac{1}{2}\chi^2\right). \tag{4.21}$$

According to Prandtl's matching principle, the remaining constant may be evaluated by reconciliation with the inner limit of $Y_n^{(j)}$. First, however, the outer expansion of Y_n^i must be made available. This can be realized by writing, for large χ,

$$(Y_n^i)^o = C_0 \frac{\Gamma\left(\frac{1}{2}\right)}{\Gamma\left(\frac{3}{2} + n - \frac{1}{2}\mathrm{i}\alpha^{-1}S\right)} (r/\sqrt{2\delta/\alpha})^{2+2n-\mathrm{i}S/\alpha}. \tag{4.22}$$

At this point, (4.22) can be matched with the inner limit of the outer solution, $Y_n^o = r^{2n+2-\mathrm{i}S/\alpha}$. The result is

$$C_0 = \pi^{-\frac{1}{2}} \Gamma(\tfrac{3}{2} + n - \tfrac{1}{2}\mathrm{i}\alpha^{-1}S)\, (2\delta/\alpha)^{1+n-\frac{1}{2}\mathrm{i}S/\alpha}. \tag{4.23}$$

Substituting back into (4.21) and reverting to the unstretched variable, one finds

$$Y_n^i(r) = \pi^{-\frac{1}{2}} \Gamma\left(\tfrac{3}{2} + n - \tfrac{1}{2}\mathrm{i}\alpha^{-1}S\right)(2\delta\alpha^{-1})^{1+n-\frac{1}{2}\mathrm{i}S/\alpha} \times \exp(-\tfrac{1}{2}\alpha\delta^{-1}r^2)\Phi\left(\tfrac{3}{2} + n - \tfrac{1}{2}\mathrm{i}\alpha^{-1}S,\ \tfrac{1}{2},\ \tfrac{1}{2}\alpha\delta^{-1}r^2\right). \tag{4.24}$$

A composite solution can thus be formed by adding to $Y_n^{(j)}$ the inner solution minus

the common limit. This combination yields

$$Y_n^c = Y_n^i + Y_n^{(j)} - (Y_n^i)^o \equiv Y_n^{(j)} + \bar{Y}_n^{(j)} = Y_n^{(j)} + \pi^{-\frac{1}{2}}\Gamma\left(\tfrac{3}{2}+n-\tfrac{1}{2}\mathrm{i}\alpha^{-1}S\right)(2\delta\alpha^{-1})^{1+n-\frac{1}{2}\mathrm{i}S/\alpha}$$
$$\times \exp(-\tfrac{1}{2}\alpha\delta^{-1}r^2)\Phi\left(\tfrac{3}{2}+n-\tfrac{1}{2}\mathrm{i}\alpha^{-1}S,\ \tfrac{1}{2},\ \tfrac{1}{2}\alpha\delta^{-1}r^2\right) - r^{2n+2-\mathrm{i}S/\alpha}, \quad (4.25)$$

where the net inner correction $\bar{Y}_n^{(j)}$ is seen to be very small, being of $O(\delta^{1+n})$. It may be shown that (4.25) mimics the exact solution in the neighbourhood of $r = 0$. However, $\bar{Y}_n^{(j)}$ is more elaborate due to the presence of special functions; it also reduces the accuracy of the solution in the outer domain, especially near the wall. Because C_0 is found by matching, it leads to an approximation that becomes increasingly more accurate asymptotically in δ. For this reason, Y_n^c becomes less precise than $Y_n^{(j)}$ in the outer region. Nonetheless, as $\delta \to 0$, Y_n^c will stand to outperform $Y_n^{(j)}$ in its ability to match both boundary conditions while yielding a value of $O(\delta^{1+n})$ at the core. In practice, since $\bar{Y}_n^{(j)} = O(\delta^{1+n})$, one can express the basic solution as $Y_n^W = Y_n^{(0)} + O(\delta)$, $\bar{Y}_n^{(j)}$ notwithstanding.

4.6. *The endpoint corrections for small and large R*

The example we have cited serves a dual purpose. First, it illustrates the relationship between exact and asymptotic forms of the solution for a test function $F = \alpha r$. More importantly, perhaps, it provides the general form of the inner solution for Berman's small and large mean-flow functions. This is due to the suitability of $F = \alpha r$, $\alpha = (\frac{3}{2}, \frac{1}{2}\pi)$ in representing the inner expansions for $F = [\frac{1}{2}r(3-r^2),\ \sin(\frac{1}{2}\pi r)]$. For example, in order to find $\bar{Y}_n^{(j)}$ for the large injection case, one must first realize that the outer solution is given by

$$Y_n^o = \lim_{\delta\to 0} Y_n^{(j)} = (\cos\theta)^{2n+2}\exp\left[\tfrac{2}{\pi}\mathrm{i}S\ln\tan\left(\tfrac{1}{4}\pi+\tfrac{1}{2}\theta\right)\right] = \left[\sin\left(\tfrac{1}{2}\pi r\right)\right]^{2n+2}$$
$$\times \exp\left[-\tfrac{2}{\pi}\mathrm{i}S\ln\tan\left(\tfrac{1}{4}\pi r\right)\right], \quad (4.26)$$

with the inner limit

$$(Y_n^o)^i = \lim_{r\to 0}\left[\sin\left(\tfrac{1}{2}\pi r\right)\right]^{2n+2}\exp\left[-\tfrac{2}{\pi}\mathrm{i}S\ln\tan\left(\tfrac{1}{4}\pi r\right)\right] = 2^{\frac{2}{\pi}\mathrm{i}S}\left(\tfrac{1}{2}\pi r\right)^{2n+2-\frac{2}{\pi}\mathrm{i}S}. \quad (4.27)$$

Insofar as $\sin(\frac{1}{2}\pi r) \sim \frac{1}{2}\pi r$ in the near-core region, the general form of the inner solution becomes identical to (4.21) with $\alpha = \frac{1}{2}\pi$. The outer limit of Y_n^i also coincides with (4.22). The only difference here is that C_0 must be found by matching (4.27) with (4.22). Thus, by setting $(Y_n^i)^o = (Y_n^o)^i$, one finds

$$C_0 = 2^{\frac{2}{\pi}\mathrm{i}S}\pi^{\frac{1}{2}+n-\frac{1}{\pi}\mathrm{i}S}\Gamma(\tfrac{3}{2}+n-\tfrac{1}{\pi}\mathrm{i}S)\delta^{1+n-\frac{1}{\pi}\mathrm{i}S}. \quad (4.28)$$

The composite solution can be constructed from (4.25) and (3.16). One finally obtains

$$Y_n^c = Y_n^i - (Y_n^i)^o + Y_n^{(j)} = 2^{\frac{2}{\pi}\mathrm{i}S}\pi^{\frac{1}{2}+n-\frac{1}{\pi}\mathrm{i}S}\Gamma\left(\tfrac{3}{2}+n-\tfrac{1}{\pi}\mathrm{i}S\right)\delta^{1+n-\frac{1}{\pi}\mathrm{i}S}$$
$$\times \exp\left(-\tfrac{1}{4}\pi\delta^{-1}r^2\right)\Phi\left(\tfrac{3}{2}+n-\tfrac{1}{\pi}\mathrm{i}S,\ \tfrac{1}{2},\ \tfrac{1}{4}\pi\delta^{-1}r^2\right) - 2^{\frac{2}{\pi}\mathrm{i}S}\left(\tfrac{1}{2}\pi r\right)^{2n+2-\frac{2}{\pi}\mathrm{i}S} + (\cos\theta)^{2n+2}$$
$$\times\exp\left(-\tfrac{1}{\pi}\delta S^2\left[\ln\tan\left(\tfrac{1}{4}\pi+\tfrac{1}{2}\theta\right)+\sec\theta\tan\theta\right]+\tfrac{2}{\pi}\mathrm{i}S\ln\tan\left(\tfrac{1}{4}\pi+\tfrac{1}{2}\theta\right)\right.$$
$$-\mathrm{i}\delta S\left\{\tfrac{1}{8\pi}\delta S\left[12\ln\tan\left(\tfrac{1}{4}\pi+\tfrac{1}{2}\theta\right)+\sec^4\theta(11\sin\theta+3\sin 3\theta)\right]\right.$$
$$\left.\left.+\left(2n+\tfrac{3}{2}\right)(\sec^2\theta-1)\right\}\right), \quad j=0. \quad (4.29)$$

The small correction gained by retaining the inner solution is illustrated in table 3 using two test functions. The composite solution has the advantage of better

https://doi.org/10.1017/S0022112009007939 Published online by Cambridge University Press

	$F = \frac{1}{2}\pi(1-y)$			$F = \cos(\frac{1}{2}\pi y)$				
y	Y_0^E	$Y_0^{(2)}$	Y_0^c	Y_0^N	$Y_0^{(2)}$	Y_0^i	$(Y_0^i)^o$	Y_0^c
0.00	1	1	0.9999678	1	1	0.4046515	0.4046571	0.9999944
0.05	−0.0558466	−0.0558466	−0.0558415	−0.7977303	−0.7977303	−2.2149878	−2.2150676	−0.7976505
0.10	−0.7918366	−0.7918366	−0.7918057	0.2960063	0.2960063	0.0946690	0.0946803	0.2959950
0.20	0.4367574	0.4367574	0.4367376	−0.6655363	−0.6655363	−0.9618275	−0.9618818	−0.6654820
0.30	0.1715711	0.1715711	0.1715570	−0.7881319	−0.7881319	1.1865032	1.1865797	−0.7882084
0.40	−0.3064925	−0.3064925	−0.3064666	−0.5652062	−0.5652062	0.3355138	0.3355507	−0.5652431
0.50	−0.2493209	−0.2493209	−0.2492890	−0.4879304	−0.4879304	−0.0568756	−0.0568754	−0.4879305
0.60	−0.1004289	−0.1004289	−0.1004110	−0.1167005	−0.1167005	0.2624337	0.2624921	−0.1167589
0.70	0.0729891	0.0729891	0.0729648	0.0281442	0.0281442	−0.0985015	−0.0985435	0.0281861
0.80	0.0227773	0.0227773	0.0227615	−0.0487533	−0.0487533	−0.0707224	−0.0707845	−0.0486912
0.90	−0.0050751	−0.0050751	−0.0050613	0.0176026	0.0176026	0.0188282	0.0188938	0.0175370
0.95	0.0011016	0.0011016	0.0010901	−0.0048594	−0.0048594	−0.0049298	−0.0049981	−0.0047911
1.00	-3.98×10^{-17}	0	-3.98×10^{-17}	-1.993×10^{-17}	0	-1.994×10^{-17}	0	-1.994×10^{-17}

TABLE 3. Type I WKB approximation with and without the inner correction Y_0^i. Here $S = 50$, $R = 10^7$ and $n = 0$. Note that the composite solution Y_0^c matches Y_0^E and Y_0^N at both ends of the interval.

approximating the exact solution near the core. Unlike $Y_0^{(2)}$, Y_0^c approaches Y_0^E and Y_0^N at both ends of the interval. However, inasmuch as the matching and subsequent determination of C_0 is based on $R \to \infty$, Y_0^c remains less accurate than $Y_0^{(2)}$ in the outer domain when R is finite. This is evident at $y = 0$ where $Y_0^c \to 1$ asymptotically in δ. Thus, as $\delta \to 0$, the precision of the composite solution is improved.

5. Multiple scales

5.1. *Strategy*

Having presented two WKB approximations and one matched asymptotic expansion for the problem at hand, attention is now turned to the method of multiple scales. In previous work by Majdalani (2001), the modified variable was left unspecified while carrying out the two-scale expansion. At the conclusion of the asymptotic analysis, physical arguments were called upon in evaluating the conceptual coordinate. These physical arguments were based on comparisons with an available WKB solution. The strategy here is different in that it precludes provisional comparisons with supplementary expansions. At present, the UST will be connected to the problem's solvability condition. The latter will be based on the principle of least singular behaviour (Van Dyke 1975).

5.2. *A generalized two-scale expansion*

To begin, we let our two fictitious coordinates be $y_0 = y$, and $y_1 = \delta s(y)$. The difference here is that $s(y)$ will remain unspecified until the solvability condition is applied. Forthwith, functions and derivatives are expanded into

$$Y_n(y_0, y_1) = Y^{(0)}(y_0, y_1) + \delta Y^{(1)}(y_0, y_1) + O(\delta^2), \quad \frac{\mathrm{d}}{\mathrm{d}y} = \frac{\partial}{\partial y_0} + \delta \frac{\mathrm{d}s}{\mathrm{d}y_0}\frac{\partial}{\partial y_1}, \quad \frac{\mathrm{d}^2}{\mathrm{d}y^2} = \frac{\partial^2}{\partial y_0^2} + O(\delta). \tag{5.1}$$

When inserted into (2.7), these expressions give rise to a sequence of partial differential equations (PDEs) at different orders in δ. For the leading and first orders, one identifies

$$\frac{\partial Y^{(0)}}{\partial y_0} - \left[2(n+1)\frac{F'}{F} + \mathrm{i}\frac{S}{F}\right] Y^{(0)} = 0, \quad Y^{(0)}(0) = 1, \quad Y'^{(0)}(1) = 0, \tag{5.2}$$

$$\frac{\partial Y^{(1)}}{\partial y_0} - \left[2(n+1)\frac{F'}{F} + \mathrm{i}\frac{S}{F}\right] Y^{(1)} = -\frac{\mathrm{d}s}{\mathrm{d}y_0}\frac{\partial Y^{(0)}}{\partial y_1} + \frac{1}{F}\frac{\partial^2 Y^{(0)}}{\partial y_0^2}. \tag{5.3}$$

Then, integration of (5.2) gives

$$Y^{(0)}(y_0, y_1) = K_1(y_1) \exp\left\{2(n+1)\ln\left[F(y_0)/F_0\right] + iS\int_0^{y_0} F^{-1}(z)\,\mathrm{d}z\right\}, \tag{5.4}$$

where K_1 awaits evaluation from the first-order equation. This multiplier can be determined in a manner to promote the least singular behaviour in Y_n. To that end, we find it unnecessary to determine $Y^{(1)}$ fully. Rather, it is sufficient to introduce a solvability condition for which an asymptotic series expansion of the form $Y^{(0)} + \delta Y^{(1)} + O(\delta)$ may be realized. This is accomplished by first introducing

$$\Lambda = \frac{Y^{(1)}(y_0, y_1)}{Y^{(0)}(y_0, y_1)}. \tag{5.5}$$

In order to determine Λ, one can multiply (5.2) by $Y^{(1)}[Y^{(0)}]^{-2}$ and subtract the result from the product of (5.3) and $[Y^{(0)}]^{-1}$. This operation yields

$$\frac{1}{Y^{(0)}}\frac{\partial Y^{(1)}}{\partial y_0} - \frac{Y^{(1)}}{[Y^{(0)}]^2}\frac{\partial Y^{(0)}}{\partial y_0} = -\frac{s'}{Y^{(0)}}\frac{\partial Y^{(0)}}{\partial y_1} + \frac{1}{FY^{(0)}}\frac{\partial^2 Y^{(0)}}{\partial y_0^2}. \tag{5.6}$$

Noting that the left-hand side is the partial derivative of Λ with respect to y_0, (5.6) can be integrated into

$$\Lambda = \frac{Y^{(1)}}{Y^{(0)}} = \int^{y_0}\left[-\frac{s'}{Y^{(0)}}\frac{\partial Y^{(0)}}{\partial y_1} + \frac{1}{FY^{(0)}}\frac{\partial^2 Y^{(0)}}{\partial y_0^2}\right]\mathrm{d}z. \tag{5.7}$$

At this point, (5.4) can be differentiated and substituted into (5.7); one finds

$$\begin{aligned}\Lambda = -\frac{s(y_0)}{K_1}\frac{\mathrm{d}K_1}{\mathrm{d}y_1} + \int^{y_0}\{&-S^2F^{-3} + 2(n+1)[F''F^{-2} + (2n+1)F'^2F^{-3}]\\ &+ \mathrm{i}S(4n+3)F'F^{-3}\}\,\mathrm{d}z = -\frac{s(y_0)}{K_1}\frac{\mathrm{d}K_1}{\mathrm{d}y_1}\\ &-S^2\times\int^{y_0}[F^{-3} - \mathrm{i}S^{-1}(4n+3)F'F^{-3} + O(S^{-2})]\,\mathrm{d}z.\end{aligned} \tag{5.8}$$

5.3. *The problem's solvability condition*

In order to promote a uniformly valid series, the ratio of $Y^{(1)}$ and $Y^{(0)}$ must be bounded $\forall y_1$. This can be accomplished by posing $\Lambda = O(1)$. Equation (5.8) becomes

$$\Lambda = -\frac{s(y_0)}{K_1}\frac{\mathrm{d}K_1}{\mathrm{d}y_1} - S^2\int^{y_0}\left[F^{-3} + \mathrm{i}S^{-1}\left(2n+\tfrac{3}{2}\right)(F^{-2})' + O(S^{-2})\right]\mathrm{d}z = O(1). \tag{5.9}$$

For arbitrary F, Λ will be bounded if and only if

$$\frac{1}{K_1(y_1)}\frac{\mathrm{d}K_1(y_1)}{\mathrm{d}y_1} = \kappa(y_1) = O(1) \quad \text{or}$$

$$K_1(y_1) = K_0\exp\left(\int\kappa\,\mathrm{d}y_1\right) = K_0\exp\left(\delta\int\kappa\,\mathrm{d}s\right). \tag{5.10}$$

On the one hand, K_0 emerges as a constant that can be determined from $Y^{(0)}(0) = 1$. On the other hand, κ appears as an auxiliary function that is self-cancelling. Moreover, when (5.10) is substituted back into (5.9), $s(y_0)$ may be deduced. The result is

$$s(y_0) = -\kappa^{-1}S^2\left\{\int^{y_0}\left[F^{-3} + \mathrm{i}S^{-1}\left(2n+\tfrac{3}{2}\right)(F^{-2})'\right]\mathrm{d}z + S^{-2}\Lambda\right\}. \tag{5.11}$$

Subsequently, since $\Lambda = O(1)$, one can put

$$\partial s/\partial y_0 = -\kappa^{-1}S^2\left\{\left[F^{-3} + \mathrm{i}S^{-1}\left(2n+\tfrac{3}{2}\right)(F^{-2})'\right] + O(S^{-2})\right\}, \tag{5.12}$$

so that, by virtue of (5.1),

$$\begin{aligned}\mathrm{d}s &= \left(\partial s/\partial y_0 + \delta s'\partial s/\partial y_1\right)\mathrm{d}y\\ &= \left(-\kappa^{-1}S^2\left\{\left[F^{-3} + \mathrm{i}S^{-1}\left(2n+\tfrac{3}{2}\right)(F^{-2})'\right] + O(S^{-2})\right\} + O(\delta)\right)\mathrm{d}y.\end{aligned} \tag{5.13}$$

This can be substituted into (5.10) to get

$$K_1(y_1) = K_0\exp\left[\delta\int\left(-S^2\left\{\left[F^{-3} + \mathrm{i}S^{-1}\left(2n+\tfrac{3}{2}\right)(F^{-2})'\right] + O(S^{-2})\right\} + O(\delta)\right)\mathrm{d}y\right]. \tag{5.14}$$

From (5.11), it becomes clear that the problem exhibits an underlying multiple-scales structure that cannot be captured by linear transformations. As such, it justifies the analyses in which the use of nonlinear coordinates is suggested (Majdalani 1998, 2001). In fact, the use of a nonlinear scaling transformation is first reported by Van Dyke (1975) in his account of Munson's treatment of the vortical layer over an inclined cone (Munson 1964). Common to these problems is the coexistence of several mechanisms involving dispersive and dissipative mechanisms. Under such circumstances, it is possible for the transitional variables to be nonlinear functions of space. In problems such as those described here, the freedom of a general transformation allows us to capture the nonlinear behaviour.

5.4. *A generalized coordinate*

Recalling that the type I distinguished limit is $\delta \sim S^{-2}$, a solution may be arrived at by substituting (5.14) back into (5.4). Using the superscript G to denote a multiple-scales solution based on a generalized coordinate, the multiple-scales result reduces to

$$Y_n^G = (F/F_0)^{2n+2} \exp\left\{-\xi \int_0^y F^{-3}\,\mathrm{d}z + \mathrm{i}\left[S\int_0^y F^{-1}\,\mathrm{d}z + \left(2n+\tfrac{3}{2}\right)S\delta\left(F_0^{-2}-F^{-2}\right)\right]\right\} + O(\delta). \quad (5.15)$$

This expression reproduces the dominant parts in Y_n^W. Despite being of the same order as (3.14), it is simpler to evaluate because it does not contain the higher order integral seen in (4.3). Furthermore, it displays the coordinate transformation required in a standard multiple-scales analysis. From (5.11), one realizes that

$$s^G \sim \int_0^y F^{-3}\,\mathrm{d}z + \mathrm{i}S^{-1}\left(2n+\tfrac{3}{2}\right)F^{-2}. \quad (5.16)$$

Having determined Y_n^G, the velocity of the travelling wave may be deduced from (2.1). One obtains

$$u_1^G(x, y, t) = \sin(\omega_m x)\,\sin(\omega_m t) - (F/F_0)\,\sin(\omega_m x F/F_0)\exp\zeta^G \sin\left(\omega_m t + \Phi^G\right), \quad (5.17)$$

where

$$\zeta^G = -\xi\int_0^y F^{-3}(z)\,\mathrm{d}z,\quad \Phi^G = -\left[S\int_0^y F^{-1}(z)\,\mathrm{d}z + \tfrac{3}{2}S\delta\left(F_0^{-2}-F^{-2}\right)\right]. \quad (5.18)$$

6. Discussion

6.1. *Error verification*

In order to verify the truncation order associated with each approximation, the maximum error evolving from Y_n^G, Y_n^W and Y_n^K can be determined from

$$E_n^A(n, S, \delta) = \max_{0\leqslant y\leqslant 1}\left|Y_n^N(y, n, S, \delta) - Y_n^A(y, n, S, \delta)\right|, \quad (6.1)$$

where Y_n^N is the numerical solution of (2.2) and Y_n^A is a given asymptotic solution for $A = \{G, W, K\}$. Following the formal test proposed by Bosley (1996), one may generate a log–log plot of E_n^A versus δ at fixed S and n. Assuming that $E_n^A(n, S, \delta) \sim \delta^\kappa$, the order of the error κ is deducible from the graph. For the first two eigenvalues, this procedure is illustrated in figure 4 where the error in each approximation is

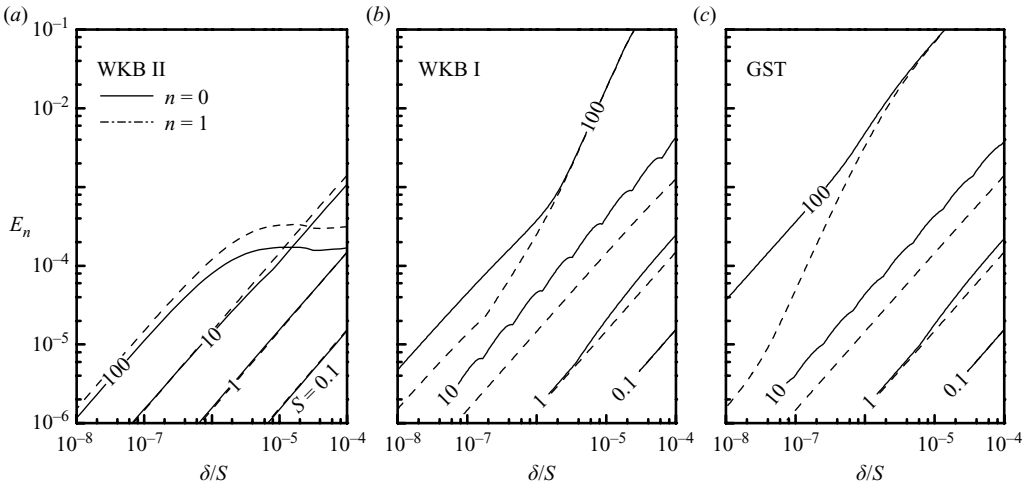

FIGURE 4. In descending level of precision, we present the errors evolving from the uniformly valid expansions of (*a*) Y^K, (*b*) Y^W and (*c*) Y^G. The test function corresponds to $F = \cos(\frac{1}{2}\pi y)$ and $n = 0, 1$.

displayed versus δ/S at constant S. This is done in the interest of clarity because error curves become too closely spaced when plotted versus δ. In all cases, the error is seen to exhibit a clear asymptotic character. Specifically, one notes that $\kappa \to 1$ as $\delta \to 0$, in compliance with a leading-order expansion. Overall, Y_n^K displays the smallest absolute error $\forall S, \delta$ and $n = 0, 1$. This can be attributed, in part, to the ability of Y_n^K to outperform other asymptotic solutions at both ends of the domain. On the other hand, both Y_n^G and Y_n^K exhibit regions of accelerated convergence in which the error increases to order 2 in some range of the operating parameters. At higher eigenvalues, the error gradually diminishes for $S \geqslant 10$ except in Y_n^K. In fact, E_n^K in figure 4(*a*) constitutes the only case for which the error increases with n, $\forall S$. It is interesting to note that all errors diminish and merge as the Strouhal number is reduced. They converge to the same value at $S = 0.1$.

6.2. *Characteristic length scales*

In a previous investigation of the oscillatory porous channel flow, the UST approximation was used wherein the space-reductive variable was left unspecified during the derivation. At the conclusion of the effort, the undetermined variable was deduced by matching the leading UST term with that of the WKB. This rationalization was based on the physical argument that exponential damping of the oscillatory wave ought to occur at the same rate irrespective of the technique used. In essence, it conformed to Prandtl's principle of matching by supplementary expansions. As a windfall, a general form for the length scale η^U could be arrived at. This relationship produced η^U explicitly for an arbitrary mean-flow function F. For example, one could write

$$\eta^U = F^3 \int_0^y F^{-3}\, \mathrm{d}z$$
$$= \begin{cases} \frac{1}{108} r(r^2-3)\left[18 - 27r^2 + 6r^4 + 2r^2(r^2-3)^2 \ln(3r^{-2}-1)\right], & \text{small } R \\ \frac{1}{\pi}\cos^3\left(\frac{1}{2}\pi y\right)\left[\ln\tan\frac{1}{4}\pi(1+y) + \sec\left(\frac{1}{2}\pi y\right)\tan\left(\frac{1}{2}\pi y\right)\right], & \text{large } R \end{cases}. \quad (6.2)$$

This result could be directly used to explain and guide the selection of inner variables in similar studies of oscillatory flows in porous channels. On the downside, it required matching with an available solution.

The shortcoming of the UST paradigm is eliminated in the GST approximation. At present, neither guesswork nor rationalization is required. In fact, specification of the scale in (5.11) is independently realized by imposing the principle of minimum singularity. From (5.11), the need for a nonlinear variable transformation is formally established. Based on (5.16), the problem's scaling functional can be determined from

$$\eta^G = \frac{F^3 \int_0^y F^{-3} \mathrm{d}z + \mathrm{i}S^{-1}\left(2n + \frac{3}{2}\right) F}{1 - \mathrm{i}S^{-1}(4n+3)F'}. \tag{6.3}$$

It may be instructive to note that η^U can be restored from η^G since $\eta^G \to \eta^U$ as $S \to \infty$ at constant n. Thus η^U represents the leading-order, parameter-free component of η^G. This also explains the ability of the UST expansion to yield a rational approximation.

6.3. *A simple test case*

The usefulness of (5.16) may be illustrated by considering $F = \alpha(1-y)$; $\alpha > 0$. Accordingly,

$$\delta \frac{\mathrm{d}^2 Y_n}{\mathrm{d}y^2} - \alpha(1-y)\frac{\mathrm{d}Y_n}{\mathrm{d}y} + [\mathrm{i}S - 2(n+1)\alpha]\, Y_n = 0. \tag{6.4}$$

Apart from the benefit of obtaining a multiple-scales solution directly from (5.15) or (5.17), the use of (5.16) enables us to identify the type of transformation needed in a standard two-variable expansion. As shown by Majdalani (1999), the corresponding equation (6.4) cannot be solved asymptotically using linear transformations. One may verify the futility of using $y_0 = y$ and any linear distortion of the form $y_1 = (1-y)\sqrt{\alpha/(2\delta)}$, $y\sqrt{\alpha/(2\delta)}$, $\delta^{-\lambda}(1-y)$, $\delta^{-\lambda}y$, $\forall\lambda$. Instead, one must resort to (5.16) and determine that the second coordinate transformation must follow

$$s^G \sim \int_0^y \alpha^{-3}(1-z)^{-3}\, \mathrm{d}z + O(S^{-1}) = \tfrac{1}{2}\alpha^{-3}\left[(1-y)^{-2} - 1\right] + O(S^{-1}). \tag{6.5}$$

Considering that constants do not affect the scaling order, the nonlinear coordinate $s^G = \frac{1}{2}\alpha^{-3}(1-y)^{-2}$ is realized. Subsequently, it can be shown that a conventional application of multiple-scales analysis with $y_0 = y$ and $y_1 = \delta s^G = \frac{1}{2}\alpha^{-3}\delta(1-y)^{-2}$ yields a uniformly valid solution that is identical to the GST result. The use of (5.16) or (6.3) can be especially helpful in treating more elaborate forms of F. At this point, it may be instructive to note that an extended form of the GST approach may be potentially employed such that the strained coordinate, y_1, is granted more freedom through the WKB-like expansion

$$y_1 = \beta^{-1}s_0 + s_1 + \beta s_2 + \beta^2 s_3 + \beta^3 s_4 + \cdots = \sum_{k=0}^{\infty} \beta^{k-1} s_k. \tag{6.6}$$

The resulting work will reproduce, after considerable effort, the WKB approximations obtained in § 3. The detail of such analysis will be the topic of a future investigation.

6.4. *Behaviour and confirmation*

Based on Bosley's test, one may also examine the maximum error E_m between u_1^A given asymptotically and u_1^N obtained numerically. Using

$$E_m^A = \max_{\substack{0 \leqslant x \leqslant l \\ 0 \leqslant y \leqslant 1}} \left|u_1^N - u_1^A\right|, \; E_m^A \sim \delta^{\kappa}, \tag{6.7}$$

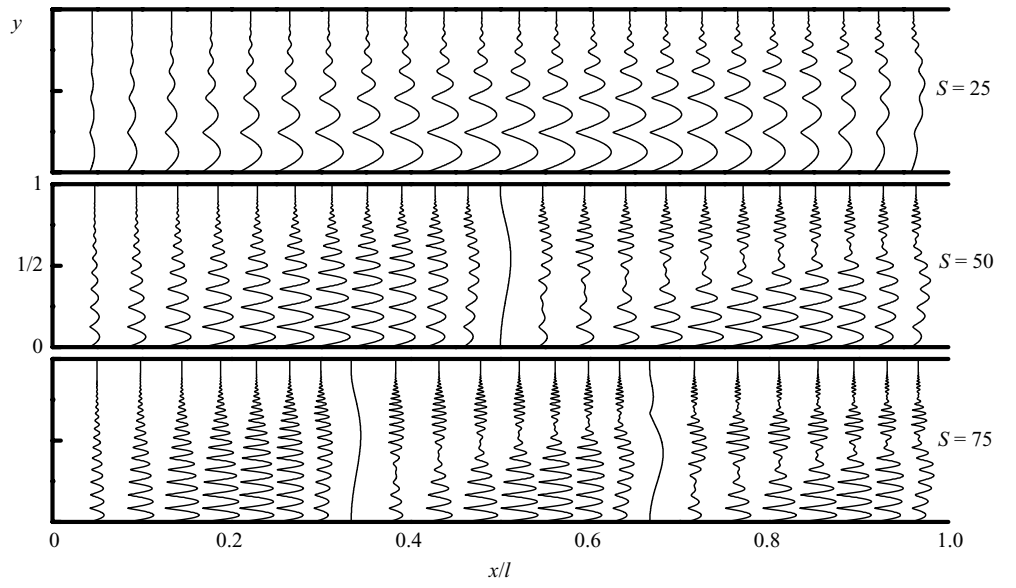

FIGURE 5. Modulus of the time-dependent velocity $u_1(x, y, t)$ for the first three oscillation modes. Results are shown at equal intervals along the channel. Here $F = \cos(\frac{1}{2}\pi y)$, $R = 4 \times 10^4$ and $S = 25m$; $m = 1, 2, 3$.

the order of the error may be calculated. Comparisons between E_m^G, E_m^W and E_m^U yield $\kappa \to 1$ consistently as $\delta \to 0$ at fixed S. According to Bosley (1996), the resulting asymptotic behaviour confirms that the solutions are legitimate, error-free approximations. Overall, we find that the smallest error evolves from E_m^K and is followed by E_m^W and E_m^G. Since E_m^A diminishes as S is reduced, these approximations remain unconditionally valid as the Strouhal number is lowered at constant δ.

The behaviour of u_1^K (or u_1^N) is illustrated in figure 5 at constant $R = 4 \times 10^4$, $F = \cos(\frac{1}{2}\pi y)$ and a typical Strouhal number of $S = 25m$. The relatively large value of the Strouhal number may be attributed to our reference velocity being based on the wall injection speed v_w, which is a small quantity when compared to the mainstream velocity used in classical acoustics. The precision at this Reynolds number causes the numerical and asymptotic solutions to become indiscernible for the given graphical resolution. As the oscillation mode number is increased, the modulus of u_1^K is seen to follow the spatial mode shape of the irrotational plane wave represented by the first member of (2.1). For the fundamental oscillation mode ($S = 25$), the modulus reaches its maximum halfway along the channel where the sinusoidal plane wave amplitude is largest. The penetration depth of the wave continues to increase in the downstream direction due to the convection of unsteady vorticity that accompanies the mean-flow for $F = \cos(\frac{1}{2}\pi y)$. For the first harmonic ($S = 50$), a sinusoidal velocity node appears at $x = \frac{1}{2}l$; this local deficit in the parallel flow component eliminates the local coupling between acoustic and rotational waves. Nonetheless, the rotational wave amplitude remains non-zero above the wall due to the downstream convection of unsteady vorticity.

The spatial evolution of the unsteady vorticity is captured in figure 6 for the first three harmonic oscillation modes, $m = 2$, 3 and 4. This is effectuated by displaying equally distributed isovorticity contours, starting with the maximum absolute values that originate at the channel wall. Using $\pm 100\,\%$ to denote the vorticity extrema that

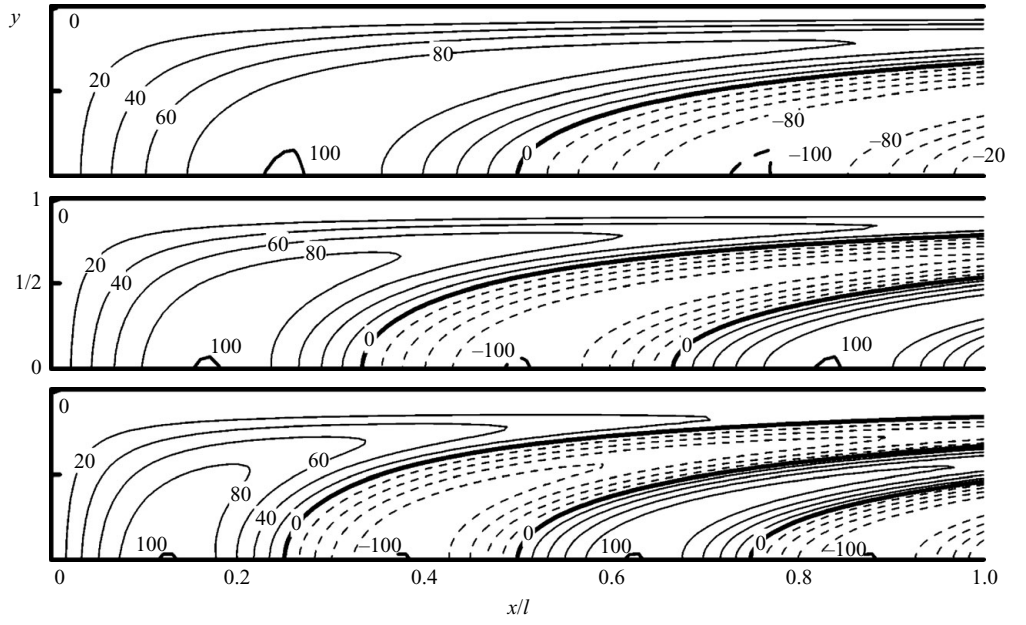

FIGURE 6. Isocontours of time-dependent vorticity for the first three harmonic oscillation modes and one instant of time. Full and broken lines denote alternating signs of vorticity that will trade back and forth with the passage of time. Here $F = \cos(\frac{1}{2}\pi y)$, $R = 4 \times 10^4$ and $S = 25m$; $m = 2, 3, 4$.

occur at the acoustic velocity antinodes, where $x/l = (2n-1)/2m$; $0 < n \leqslant m$; $n \in \mathbb{N}$, contours of constant vorticity are shown in decrements of 20 %. Their thumbprints illustrate the downstream convection and depreciation of unsteady vorticity due to the combined effects of mean-flow motion, acoustic driving at the wall, and viscous damping. They are shown in figure 6 for typical values of the control parameters. Given the alternating directions of particle rotation at different oscillation modes, some interesting features may be observed including the emergence of $(m-1)$ lines of zero unsteady vorticity. These 'irrotational' streaklines originate at the acoustic velocity nodes where surface coupling is absent. Thus, starting at $x/l = n/m$; $n < m$, these demarcation lines partition the channel into m regions of counter-rotating vorticity. In the interest of clarity, we switch from full lines to broken lines as unsteady vorticity switches direction.

The effect of decreasing the wall injection velocity is examined in figure 7 where the wave modulus is displayed for the first oscillation mode shape. By fixing the wave frequency and fluid viscosity, reducing the injection velocity by one order of magnitude is seen to shorten the spatial wavelength in the wall-normal direction. The penetration depth is also reduced. These trends are typical of those reported in the literature.

In figure 8, the axially travelling wave u_1 is compared to the numerical solution for the first fundamental oscillation mode, $F = \cos(\frac{1}{2}\pi y)$, and $x = \frac{1}{2}l$ (midway along the channel). Interestingly, by holding $\xi = 5$, the Strouhal number may be varied over a wide range of frequencies without affecting the thickness of the rotational region. It is clear that the agreement between numerics and asymptotics improves with successive increases in the Strouhal number despite the highly oscillatory nature of the solution and the marked reduction in spatial wavelength. The observed agreement reflects the

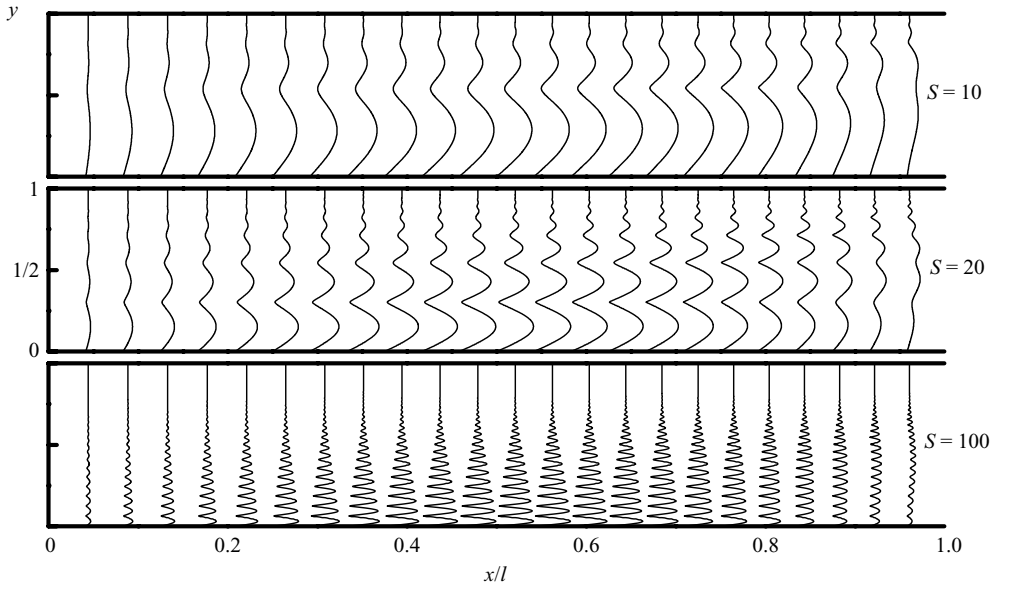

FIGURE 7. Modulus of the time-dependent velocity $u_1(x, y, t)$ for the first oscillation mode assuming constant frequency and viscosity. By holding $\varepsilon = \nu/(\omega h^2) = 10^{-6}$, the wall injection velocity is reduced, from top to bottom, by one order of magnitude. Here $F = \cos(\frac{1}{2}\pi y)$.

precision entailed in the perturbative approximations and their usefulness in disclosing keystone parameters such as ξ. This parameter plays a significant role in controlling the wave's depth of penetration and could not have been identified except through the proper use of asymptotics (Majdalani 1995).

7. Conclusions

The search for a multiple-scales solution of the oscillatory channel flow problem was initiated in 1998 due to its relevance to instability analysis. The failure of linear coordinate transformations prompted the quest for a nonlinear composite scale. By devising a space-reductive transformation in the form of a composite variable, one could reproduce the modified scales in their regions of validity. This required conjecture and careful identification of the transitional variables before constructing a composite scale. By implementing a two-variable expansion that made use of this composite scale, a uniformly valid approximation was obtained. Later, Majdalani (2001) attempted a reverse methodology. This time, the coordinate transformation was kept unspecified during the expansion. In the process, the leading-order term based on the undetermined functional was compared to a WKB solution of type I. Then, matching leading-order terms yielded the undetermined transformation. The resulting UST approximation served four objectives: (*a*) it confirmed the nonlinearity of the scales; (*b*) it provided a more formal alternative that is separately arrived at; (*c*) it reduced the amount of guesswork and subjectivity involved in the selection of inner scales and (*d*) it illustrated Prandtl's principle that proposes matching with supplementary expansions. However, by relying on the existence of a supplementary approximation, the UST expansion became limited to problems for which a procedural substitution could be entertained. This issue is circumvented in the present study where the transformation is obtained directly from the problem's solvability condition and

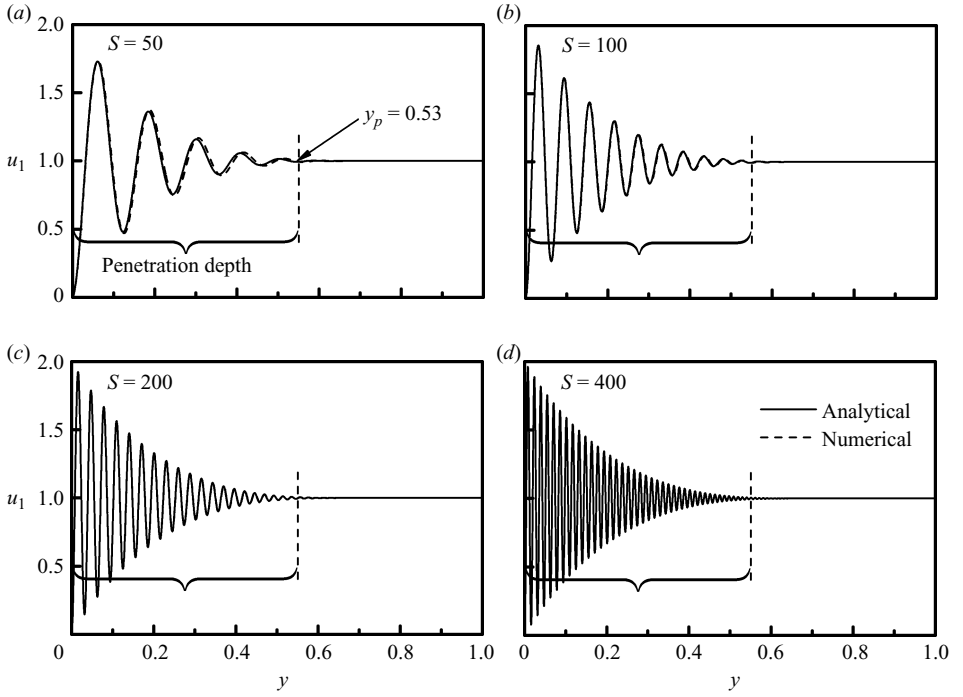

FIGURE 8. Analytical GST (full lines) and numerical (broken) solutions of the axially travelling wave for $F = \cos(\frac{1}{2}\pi y)$, $\xi = 5$, $m = 1$, $\omega_m t = \pi/2$, $x/l = 0.5$, and a Strouhal number of (*a*) $S = 50$, (*b*) 100, (*c*) 200 and (*d*) 400. By fixing ξ, the penetration depth of the travelling wave remains constant at any axial location regardless of the wall injection velocity, viscosity, or frequency of oscillations. The agreement between numerics and asymptotics continues to improve with successive increases in the Strouhal number despite the highly oscillatory nature of the solution and the radical reduction in spatial wavelength.

the principle of minimum singularity. By ensuring boundedness between successive perturbation orders, an improved expression is derived from which the UST form is restored at leading order.

Apart from being independently formulated, the GST approximation exhibits four interesting features: (*a*) it is compact and straightforward to express in closed form; (*b*) it clearly displays the physical characteristics that control the solution; (*c*) it unravels the necessary coordinate transformation without resorting to guesswork or supplementary functions and (*d*) it stems from the problem's mathematical stipulation for least singular behaviour. Furthermore, the GST approximation follows the fundamental procedural step of multiple-scales theory, namely, that of transforming the governing ODE into pairs of PDEs. Its uniqueness stands in (i) retaining a nonspecific scale until the basic solution is obtained; (ii) applying a fundamental principle to ensure boundedness between successive expansion terms and (iii) disclosing the key transformation at the conclusion of the analysis. It may be useful to add the GST's ability to provide the unique scales that, when used in a standard multiple-scales expansion, produce a result similar to that of the WKB of type I.

Particular to this investigation, two essential forms of the WKB solution are derived and presented to arbitrary order. The new type II solution is especially useful in being unconditionally valid at all orders. However, the increased algebraic complexity that accompanies type II can, in some applications, require numerical evaluation.

The type I solution is simpler but requires a small-amplitude correction in higher order representations. Incidentally, the appearance of a near-core boundary layer is consistent with conventional theory of laminar injection-driven flows.

By way of verification, several examples are offered through which the newly developed asymptotic expansions are extensively tested. Having established the accuracy of the individual eigensolutions in the wall-normal direction, the complete expression for the axially travelling wave is deduced, characterized and compared to its numerical solution.

This project was funded by the National Science Foundation through grant No. CMMI-0353518, Dr Eduardo A. Misawa, Program Director. I am thankful for the constructive reports received from the anonymous referees and for the timely assistance of Joshua W. Batterson in addressing the final round of review comments. I also wish to acknowledge a valuable technical exchange with Professor Sjoerd W. Rienstra concerning the nature of the GST.

Appendix A. Vortico-acoustic wave equation in a porous channel

The Helmholtz vector decomposition theorem enables us to synthesize the time-dependent disturbances in a porous channel from two parts: a curl-free, irrotational vector and a divergence-free, vortical component. Using the circumflex and tilde to denote either acoustic or solenoidal fields, the travelling wave in a channel may be written as $\mathbf{u}_1 = \hat{\mathbf{u}} + \tilde{\mathbf{u}}$. This subdivision of roles may be substituted into the linearized Navier–Stokes equations at the first order in the perturbed pressure wave amplitude. Forthwith, two sets of responses may be extracted for the acoustic and rotational motions. On the one hand, the irrotational set collapses into

$$\partial^2 \hat{p}/\partial t^2 - \nabla^2 \hat{p} = O(M_w);\ M_w \equiv v_w/a_s, \tag{A 1}$$

or

$$\hat{p}\,(x,t) = \cos(\omega_m x)\exp(-\mathrm{i}\omega_m t) + O(M_w), \tag{A 2}$$

$$\hat{u}\,(x,t) = \mathrm{i}\,\sin(\omega_m x)\exp(-\mathrm{i}\omega_m t) + O(M_w), \tag{A 3}$$

where $\hat{p}$ is the acoustic pressure and $\omega_m = \omega h/a_s = m\pi/l$ is the dimensionless wavenumber assuming rigid wall boundary conditions and axial oscillations in a channel with $l \gg 1$. On the other hand, the rotational response yields

$$\nabla \cdot \tilde{\mathbf{u}} = 0, \tag{A 4}$$

$$\partial \tilde{\mathbf{u}}/\partial t = -M_w\,[\nabla(\tilde{\mathbf{u}}\cdot\mathbf{u}_0) - \tilde{\mathbf{u}}\times\nabla\times\mathbf{u}_0 - \mathbf{u}_0\times\nabla\times\tilde{\mathbf{u}}] - \bar{R}^{-1}\nabla\times\nabla\times\tilde{\mathbf{u}};\quad \bar{R}\equiv a_s h/\nu. \tag{A 5}$$

Being interested in longitudinal wave motions, the no-slip condition may be invoked to impose a vanishing velocity parallel to the porous wall. Furthermore, assuming symmetry about the midsection plane, one can put

$$u_1(x,\ 0) = \hat{u}(x,\ 0) + \tilde{u}(x,\ 0) = 0, \tag{A 6}$$

$$\partial u_1(x,\ 1)/\partial y = 0. \tag{A 7}$$

Letting $\tilde{\mathbf{u}}(x,y,t) = \bar{\mathbf{u}}(x,y)\exp(-\mathrm{i}\omega_m t)$, (A 4)–(A 5) may be expressed as

$$\nabla \cdot \bar{\mathbf{u}} = 0, \tag{A 8}$$

$$\mathrm{i}\bar{\mathbf{u}} = \sigma\,[\nabla(\bar{\mathbf{u}}\cdot\mathbf{u}_0) - \bar{\mathbf{u}}\times\nabla\times\mathbf{u}_0 - \mathbf{u}_0\times\nabla\times\bar{\mathbf{u}}] + \varepsilon\nabla\times\nabla\times\bar{\mathbf{u}}. \tag{A 9}$$

Subsequently, with $\bar{v}/\bar{u} = O(M_w)$, the axial component of (A9) reduces to

$$\mathrm{i}\bar{u} = \sigma\left[\frac{\partial}{\partial x}(\bar{u}u_0) + v_0\frac{\partial \bar{u}}{\partial y}\right] - \varepsilon\frac{\partial^2\bar{u}}{\partial y^2} + O(M_w). \tag{A 10}$$

At the porous wall, the dynamic coupling with the acoustic wave requires setting $\bar{u}(x,\,0) = -\mathrm{i}\sin(\omega_m x)$. Then taking Berman's similarity form $(u_0, v_0) = (-xF', F)$ for the mean-flow and $\bar{u}(x, y) = \sum c_n x^{\lambda_n} Y_n(y)$ as a linear solution to (A 10), one finds $\lambda_n = 2n + 1,\ n \in$. The rotational wave contribution becomes

$$\tilde{u}(x, y) = -\mathrm{i}\sum_{n=0}^{\infty}\frac{(-1)^n(\omega_m x)^{2n+1}}{(2n+1)!}Y_n(y)\exp(-\mathrm{i}\omega_m t), \tag{A 11}$$

where each Y_n is left to be determined from

$$\varepsilon\frac{\mathrm{d}^2Y_n}{\mathrm{d}y^2} - \sigma F\frac{\mathrm{d}Y_n}{\mathrm{d}y} + \left[\mathrm{i} + 2\sigma(n+1)F'\right]Y_n = 0, \quad 0 \leqslant y \leqslant 1, \tag{A 12}$$

with

$$Y_n(0) = 1 \text{ (no-slip at the wall), and } Y_n'(1) = 0 \text{ (core symmetry).} \tag{A 13}$$

This completes our cursory derivation of (2.1) and (2.2).

Appendix B. Exact Kummer solution

Using $F = \alpha(1 - y)$ and $\alpha = (\frac{3}{2}, \frac{1}{2}\pi)$, (2.7) becomes

$$\delta\frac{\mathrm{d}^2Y_n}{\mathrm{d}y^2} - \alpha(1-y)\frac{\mathrm{d}Y_n}{\mathrm{d}y} + [\mathrm{i}S - 2(n+1)\alpha]Y_n = 0. \tag{B 1}$$

At this point, a double transformation of the type

$$\chi = (1-y)\sqrt{\alpha/\delta}, \quad Y_n = \exp(-\tfrac{1}{4}\chi^2)f(\chi), \tag{B 2}$$

leads to

$$f_{\chi\chi} + \left(p + \tfrac{1}{2} - \tfrac{1}{4}\chi^2\right)f = 0,\ p = -2n - 3 + \mathrm{i}\alpha^{-1}S. \tag{B 3}$$

The general solution is a linear sum of parabolic cylinder functions, namely,

$$Y_n(\chi) = \exp\left(-\tfrac{1}{4}\chi^2\right)\left[c_1 D_p(\chi) + c_2 D_p(-\chi)\right]. \tag{B 4}$$

Due to $\Re(p) < 0$, application of the symmetry condition at the core yields $c_1 = c_2$. Hence, one can put

$$Y_n(\chi) = C_1\exp(-\tfrac{1}{2}\chi^2)\Phi\left[n + \tfrac{3}{2} - \tfrac{1}{2}\mathrm{i}\alpha^{-1}S,\ \tfrac{1}{2},\ \tfrac{1}{2}\chi^2\right], \tag{B 5}$$

where Φ denotes a Kummer function. The remaining constant may be determined by applying the condition at the outer wall. One finds $C_1 = \exp(\frac{1}{2}\alpha\delta^{-1})\Phi^{-1}(n + \frac{3}{2} - \frac{1}{2}\mathrm{i}\alpha^{-1}S,\ \frac{1}{2},\ \frac{1}{2}\alpha\delta^{-1})$. It follows that

$$Y_n^E = \exp\left[\tfrac{1}{2}\alpha\delta^{-1}y(2-y)\right]\frac{\Phi\left[n + \frac{3}{2} - \frac{1}{2}\mathrm{i}\alpha^{-1}S,\ \frac{1}{2},\ \frac{1}{2}\alpha\delta^{-1}(1-y)^2\right]}{\Phi\left(n + \frac{3}{2} - \frac{1}{2}\mathrm{i}\alpha^{-1}S,\ \frac{1}{2},\ \frac{1}{2}\alpha\delta^{-1}\right)}. \tag{B 6}$$

REFERENCES

Abramowitz, M. & Stegun, I. A. 1964 *Handbook of Mathematical Functions*. National Bureau of Standards.

Barron, J., Majdalani, J. & Van Moorhem, W. K. 2000 A novel investigation of the oscillatory field over a transpiring surface. *J. Sound Vib.* **235**, 281–297.

Berman, A. S. 1953 Laminar flow in channels with porous walls. *J. Appl. Phys.* **24**, 1232–1235.

Berman, A. S. 1958 Effects of porous boundaries on the flow of fluids in systems with various geometries. *Proceedings of the Second United Nations Intl Conf. on the Peaceful Uses of Atomic Energy*, Geneva, Switzerland. P/720 vol. 4, pp. 351–358.

Bosley, D. L. 1996 A technique for the numerical verification of asymptotic expansions. *SIAM Rev.* **38**, 128–135.

Brown, R. S., Blackner, A. M., Willoughby, P. G. & Dunlap, R. 1986 Coupling between acoustic velocity oscillations and solid propellant combustion. *J. Propul. Power* **2**, 428–437.

Casalis, G., Avalon, G. & Pineau, J.-P. 1998 Spatial instability of planar channel flow with fluid injection through porous walls. *Phys. Fluids* **10**, 2558–2568.

Dunlap, R., Blackner, A. M., Waugh, R. C., Brown, R. S. & Willoughby, P. G. 1990 Internal flow field studies in a simulated cylindrical port rocket chamber. *J. Propul. Power* **6**, 690–704.

Fabignon, Y., Dupays, J., Avalon, G., Vuillot, F., Lupoglazoff, N., Casalis, G. & Prévost, M. 2003 Instabilities and pressure oscillations in solid rocket motors. *Aerosp. Sci. Technol.* **7**, 191–200.

Griffond, J. 2002 Receptivity and aeroacoustic resonance in channels with blowing walls. *Phys. Fluids* **14**, 3946–3962.

Ma, Y., Van Moorhem, W. K. & Shorthill, R. W. 1991 Experimental investigation of velocity coupling in combustion instability. *J. Propul. Power* **7**, 692–699.

Majdalani, J. 1995 *Improved Flowfield Models in Rocket Motors and the Stokes Layer with Sidewall Injection*, Ph.D. Dissertation, University of Utah.

Majdalani, J. 1998 A hybrid multiple scale procedure for boundary layers involving several dissimilar scales. *J. Appl. Math. Phys. (ZAMP)* **49**, 849–868.

Majdalani, J. 1999 Vortical and acoustical mode coupling inside a two-dimensional cavity with transpiring walls. *J. Acoust. Soc. Am.* **106**, 46–56.

Majdalani, J. 2001 The oscillatory channel flow with arbitrary wall injection. *J. Appl. Math. Phys. (ZAMP)* **52**, 33–61.

Majdalani, J. & Flandro, G. A. 2002 The oscillatory pipe flow with arbitrary wall injection. *Proc. R. Soc. Lond.* A **458**, 1621–1651.

Majdalani, J. & Rienstra, S. W. 2002 Two asymptotic forms of the rotational solution for wave propagation inside viscous channels with transpiring walls. *Q. J. Mech. Appl. Math.* **55**, 141–162.

Majdalani, J. & Van Moorhem, W. K. 1998 Improved time-dependent flowfield solution for solid rocket motors. *AIAA J.* **36**, 241–248.

Munson, A. G. 1964 The vortical layer on an inclined cone. *J. Fluid Mech.* **20**, 625–643.

Richardson, E. G. & Tyler, E. 1929 The transverse velocity gradient near the mouths of pipes in which an alternating or continuous flow of air is established. *Proc. R. Soc. Lond.* A **42**, 1–15.

Terrill, R. M. 1965 Laminar flow in a uniformly porous channel with large injection. *Aeronaut. Q.* **16**, 323–332.

Terrill, R. M. 1973 On some exponentially small terms arising in flow through a porous pipe. *Q. J. Mech. Appl. Math.* **26**, 347–354.

Ugurtas, B., Avalon, G., Lupoglazoff, N., Vuillot, F. & Casalis, G. 2000 Stability and acoustic resonance of internal flows generated by side injection. In *Solid Propellant Chemistry, Combustion, and Motor Interior Ballistics* (ed. V. Yang, T. B. Brill & W.-Z. Ren), vol. 185, pp. 823–836. AIAA Progress in Astronautics and Aeronautics.

Van Dyke, M. 1975 *Perturbation Methods in Fluid Mechanics.* The Parabolic Press.

Yuan, S. W. 1956 Further investigation of laminar flow in channels with porous walls. *J. Appl. Phys.* **27**, 267–269.